Available online at www.sciencedirect.com
ScienceDirect
Journal of Asian Earth Sciences 33 (2008) 155–176
Journal of Asian Earth Sciences
www.elsevier.com/locate/jaes

# Geochemical and mantle-like isotopic (Nd, Sr) composition of the Baklan Granite from the Muratdağı Region (Banaz, Uşak), western Turkey: Implications for input of juvenile magmas in the source domains of western Anatolia Eocene–Miocene granites

M. Selman Aydoğan [a,*], Hakan Çoban [b], Mustafa Bozcu [c], Ömer Akıncı [d]

[a] Department of Geological Engineering, Balıkesir University, TR-10145 Balıkesir, Turkey
[b] Department of Geological Engineering, Süleyman Demirel University, TR-032260 Isparta, Turkey
[c] Department of Geological Engineering, Çanakkale Onsekiz Mart University, TR-17020 Çanakkale, Turkey
[d] Havacı Bnb. Mehmet Sokak 9/12 Bostancı TR-34744 İstanbul, Turkey

Received 1 November 2005; received in revised form 12 September 2006; accepted 9 October 2006

**Abstract**

The (late syn)- post-collisional magmatic activities of western and northwestern Anatolia are characterized by intrusion of a great number of granitoids. Amongst them, Baklan Granite, located in the southern part of the Muratdağı Region from the Menderes Massif (Banaz, Uşak), has peculiar chemical and isotopic characteristics. The Baklan rocks are made up by K-feldspar, plagioclase, quartz, biotite and hornblende, with accessory apatite, titanite and magnetite, and include mafic microgranular enclaves (MME). Chemically, the Baklan intrusion is of sub-alkaline character, belongs to the high-K, calc-alkaline series and displays features of I-type affinity. It is typically metaluminous to mildly peraluminous, and classified predominantly as granodiorite in composition. The spider and REE patterns show that the rocks are fractionated and have small negative Eu anomalies ($Eu/Eu^* = 0.62–0.86$), with the depletion of Nb, Ti, P and, to a lesser extent, Ba and Sr. The pluton was dated by the K–Ar method on the whole-rock, yielded ages between $17.8 \pm 0.7$ and $19.4 \pm 0.9$ Ma (Early Miocene). The intrusion possesses primitive low initial $^{87}Sr/^{86}Sr$ ratios (0.70331–0.70452) and negative $\varepsilon_{Nd(t)}$ values ($-5.0$ to $-5.6$). The chemical contrast between evolved Baklan rocks ($SiO_2$, 62–71 wt.%; Cr, 7–27 ppm; Ni, 5–11 ppm; Mg#, 45–51) and more primitive clinopyroxene-bearing monzonitic enclaves ($SiO_2$, 54–59 wt.%; Cr, 20–310 ppm; Ni, 10–70 ppm; Mg#, 50–61) signifies that there is no co-genetic link between host granite and enclaves. The chemical and isotopic characteristics of the Baklan intrusion argue for an important role of a juvenile component, such as underplated mantle-derived basalt, in the generation of the granitoids. Crustal contamination has not contributed significantly to their origin. However, with respect to those of the Baklan intrusion, the generation of the (late syn)- post-collisional intrusions with higher Nd(t) values from the western Anatolia require a much higher amount of juvenil component in their source domains.


*Keywords:* Baklan Granite; I-type; Mantle input; Juvenile crust; Muratdağı Region; Uşak; Western Anatolia

## 1. Introduction

Granite is an important and characteristic component of continental crust. Recent studies on granite petrology revealed that diverse geodynamic processes, such as crustal thickening as a consequences of continental collision, development of lower juvenile crust via input of mantle-derived magmas, and lithospheric thinning and asthenospheric mantle upwelling (e.g. Snyder et al., 1996; Chen and Jahn, 1998, 2004; Jahn et al., 2000; Chen et al., 2000, 2002; Hu et al., 2000; Wu et al., 2000, 2003; Topuz et al., 2005; Arslan and Aslan, 2006; Zhai et al., 2007; Mo

* Corresponding author. Tel.: +90 266 612 11 94; fax: +90 266 612 12 57.
*E-mail address:* selmanbaklan@hotmail.com (M.S. Aydoğan).

1367-9120/$ - see front matter © 2007 Elsevier Ltd. All rights reserved.
doi:10.1016/j.jseaes.2006.10.007

et al., in press; Karsli et al., 2007; Boztuğ et al., 2007) leave geochemical imprints in enclave and host rock compositions of the granitic bodies. Drastic change in tectonics from a compressive to extensional processes, or a large-scale uplift and thinning, may cause compositional difference in granitic magmas (e.g. Wu et al., 2000; Dias et al., 2002; Mendes and Dias, 2004; Karsli et al., 2007). The variably mixed sources from both underplated basaltic rocks and crustal components in orogenic settings are also their most characteristic feature (e.g. Central Asian Orogenic Belt, Sengor et al., 1993; Wu et al., 2000; NW Iberian Peninsula, Mendes and Dias, 2004; NE Pontide, Karsli et al., 2007). Such geodynamic and magmatic patterns during the Late Crecateous–Late Tertiary period have also been reported for the western Anatolian (late syn)- post-collisional settings including numerous calc-alkaline granitic intrusions and their contemporary volcanic associations (Figs. 1 and 2) (Bingöl et al., 1982; Juteau et al., 1986; Güleç, 1991; Yılmaz, 1997; Altunkaynak and Yılmaz, 1998; Karacık and Yılmaz, 1998; Delaloye and Bingöl, 2000; Pe-Piper and Piper, 2001; Albayrak, 2003; Işık et al., 2004a,b; Köprübaşı and Aldanmaz, 2004; Aydoğan, 2006; Altherr and Siebel, 2002; Karacık et al., 2007). Amongst these igneous activities, the Baklan Granite (ca. $3 \times 4$ km) is only one of these plutonic rocks. It is well exposed in the southern part of the Muratdağı Region, situated in northeastern end of the Menderes Massif (SW Anatolia), a large elongate metamorphic complex in western Anatolia (cf. Bozkurt, 2001b). The Baklan Granite is a post-collisional I-type granitoid.

Here, we present new geochemical and isotopic (Sr, Nd) data for the Baklan Granite, together with the composition of its enclaves, to better understand the nature of the source domains of (late syn)- post-collisional I-type calc-alkaline granitoids from western Anatolia.

## 2. Regional geological setting

Anatolia (Turkey) is an important east–west-trending component of the Alpine–Himalayan orogenic system which marks the boundary between Gondwana to the south and Laurasia to the north. The tectonic history of Anatolia is primarily linked to the continental collision between the Eurasian and Arabian plates along the Bitlis–Zagros Suture Zone. The collision resulted in crustal thickening (regional uplift; ≈ up to 2 km) and shortening in eastern Anatolia during Middle to Late Miocene times (e.g. McKenzie, 1972, 1978; Dewey et al., 1973, 1986; Şengör, 1980; Sengör and Yılmaz, 1981) (Fig. 1). The collisional processes in the east affected the western Anatolia, as well. With the closure of the Izmir–Ankara–Erzincan Ocean, the Tauride–Anatolide Platform collided with the Sakarya continent along the Izmir–Ankara–Erzincan Suture Zone during the Palaeocene time (e.g. Sengör and Yılmaz, 1981). This collisional episode also caused a north–south crustal shortening and intra-

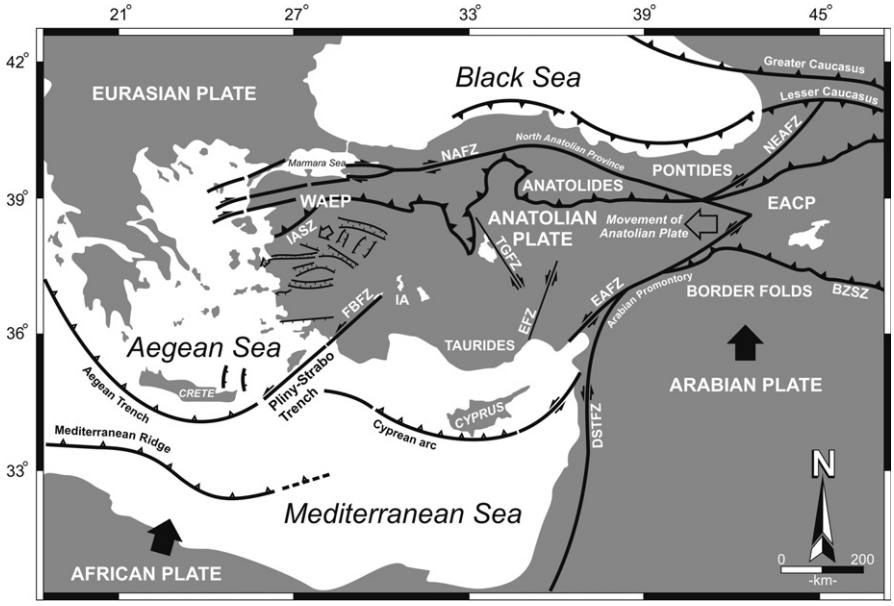


Fig. 1. Simplified structural sketch map of Turkey showing the distribution of major tectonic elements and suture zones (modified from Sengör et al., 1985; Barka, 1992; Bozkurt, 2001a). *Abbreviations:* IASZ: Izmir–Ankara–Erzincan Suture Zone, BZSZ: Bitlis–Zagros Suture Zone, DSTFZ: Dead Sea Transform Fault Zone, EAFZ: East Anatolian Fault Zone, FBFZ: Fethiye-Burdur Fault Zone, FBFZ: Fethiye-Burdur Fault Zone, NAFZ: North Anatolian Fault Zone, EFZ: Ecemiş Fault Zone, TGFZ: Tuz Gölü Fault Zone, IA: Isparta Angle, EACP: East Anatolian Contractional Province, WAEP: West Anatolian Extentional Province. Heavy lines with arrows are strike-slip faults. The arrows show the relative movement sense. Heavy lines with filled triangles show a major fold and thrust belt. Heavy lines with open triangles indicate an active subduction zone, its polarity indicated by the tip of small triangles. Bold filled arrows show relative movement direction of Arabian and African plates. Open arrows indicate westward motion of Anatolian Plate. The heavy lines with hachures indicating down-thrown side show normal faults and graben fields in western Anatolia.

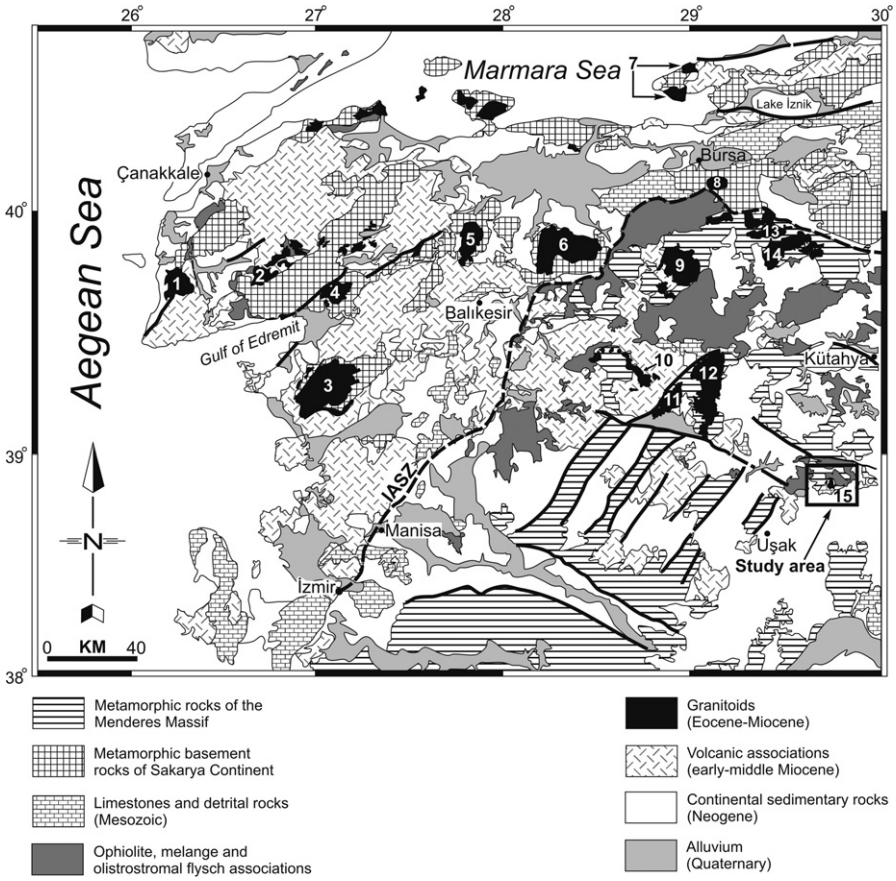


Fig. 2. Geological sketch map showing distribution of the Eocene–Miocene granitic plutons and the other rock units in western and northwestern Anatolia (modified from Bingöl, 1989; Genç, 1998). Key to numbers (from west to east): (1) Kestanbol pluton, (2) Evciler pluton, (3) Kozak granodiorite, (4) Eybek granodiorite, (5) Ilıca granodiorite, (6) Çataldağ granodiorite, (7) Fıstıklı granite, (8) Uludağ granite, (9) Orhaneli granodiorite, (10) Alaçam pluton, (11) Koyunoba pluton, (12) Eğrigöz pluton, (13) Topuk granodiorite, (14) Göynükbelen granite and (15) Baklan Granite (this work).

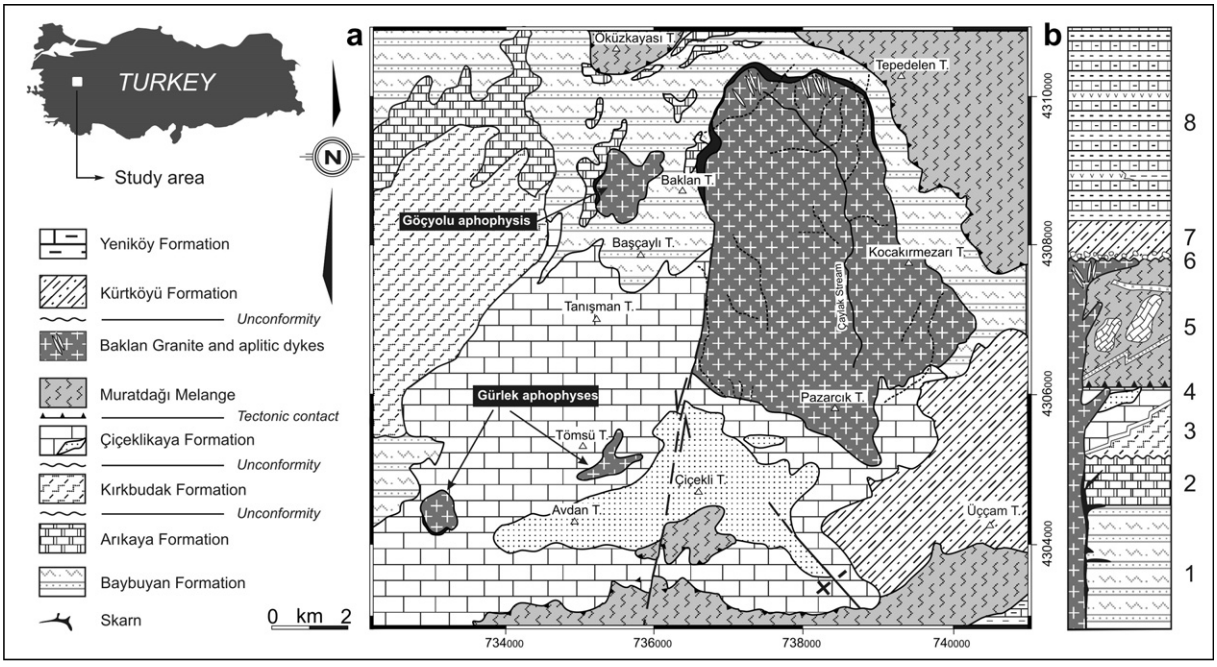


Fig. 3. (a) Geological map of southern section of Muratdağı Region (b) Generalized tectonostratigraphic column of the study area (1) Baybuyan Formation (Palaeozoic), (2) Arıkaya Formation (Palaeozoic), (3) Kırkbudak Formation (Upper-Triassic), (4) Çiçeklikaya Formation (Jurassic), (5) Muratdağı Melange (Cretaceous), (6) Baklan Granite (Middle-Lower Miocene), (7) Kürtköyü Formation (Lower Miocene), (8) Yeniköy Formation (Middle-Miocene).

crustal deformation (e.g. Sengör and Yılmaz, 1981; Okay et al., 1996, 2001). From Oligocene to middle Miocene, continental extension, due to combined effect of gravitational collapse and southward retreat of the Aegean arc, reduced the Aegean continental crust from 50 km to a mean value of 25 km at the scale of the whole Aegean (e.g. Tirel et al., 2004). The Palaeocene–Oligo-Miocene period in western Anatolia was characterized by a drastic tectonic change from collision to extension. Special emphasis has been given to the (late Oligocene)–Early Miocene post-orogenic extension (e.g. Bozkurt, 2001a,b, 2002; Işık et al., 2004a,b; Catlos and Çemen, 2005; Bozkurt and Mittwede, 2005; Emre and Sözbilir, 2007; Kaya et al., 2007). Eocene–Early Oligocene period was probably corresponds the relaxation phase of last stage of collision. In general, intense magmatic activities took place (e.g. Yılmaz, 1997; Pe-Piper and Piper, 2001; Aldanmaz, 2006; Altunkaynak, 2007; Ersoy and Helvacı, 2007; Karacık et al., 2007), following the northern subduction of the Neotethys ocean (Sengör and Yılmaz, 1981).

### 2.1. Local geological setting

The Muratdağı Region, comprising a complex mosaic of metamorphics, plutonics, ophiolitic remnants (mélange), platform-type carbonates and Neogene units, is located in the western Anatolia where young granitic and volcanic rocks are widespread (Fig. 2). A brief explanation about geological setting of the study area is given below, and stratigraphical nomenclature of lithological units are taken from Bingöl (1977), Ercan et al. (1978) and Akdeniz and Konak (1979) (Fig. 3a and b).

In the Muratdağı Region, the Menderes Massif is represented by a metasedimentary sequence. The Baybuyan Formation of Palaeozoic age, which is composed of alternation of marble, schists and quartzites, forms the lower part of the stratigraphic section of the massif (Günay et al., 1986; Güngör and Erdoğan, 2002). Based on Rb/Sr isotopic data, Bingöl (1977) postulated an age of metamorphism at $127 \pm 11$ Ma. The Baybuyan Formation is overlain conformably by the Arıkaya Formation. Upper-Triassic aged Kırkbudak Formation overlying Arıkaya Formation is dominantly composed of meta-pebblestone, meta-sandstone and limestone. The series continues with a Jurassic Çiçeklikaya Formation, which is mainly characterized by a thick-bedded dolomitized and silicified limestone (Akdeniz and Konak, 1979; Günay et al., 1986). All these units are overthrust by the Muratdağı Mélange (Fig. 3a and b) consisting mainly of mafic and ultramafic rocks, and large limestone blocks and marbles of Cretaceous age. The mafic and ultramafic rocks contain serpentinized harzburgite, gabbro, spilitic basalt and diabase. Bingöl (1977) pointed out that the emplacement age of the Muratdağı Mélange is about $70 \pm 3$ Ma. The Baklan Granite intruded into (as also aphophyzes) all these formations (mentioned above), and thermally affected them in contact zones. The Kürtköyü Formation (Lower Miocene) consists of gravels derived from the earlier formations (Ercan et al., 1978, p. 100), and discordantly overlies the Muratdağı Mélange and Çiçeklikaya Formation in southeastern part of the area. The Kürtköyü Formation is covered by the Yeniköy Formation which is composed mainly of sandstone, mudstone, siltstone, marl and clay-plaquette limestones (see Fig. 3a and b for detail).

## 3. Analytical techniques

More than 200 samples were collected from the Baklan Granite. The exact co-ordinates of our sampling sites are given in Table 1. More precise locations are plotted on

Table 1
Location and co-ordinates of the representative samples from the Baklan Granite

| Location | Outcrop | Sample | Co-ordinates | |
|---|---|---|---|---|
| | | | Latitude (N) | Longitude (E) |
| Kozakırmezarı | N of the Çiçekli Hill, E of the Pazarcık Hill | MBG-2 | 38°52′13″ | 29°45′23″ |
| Kozakırmezarı | SW of Kocakırmezarı Hill, on the road of Baklan Hill | MBG-3 | 38°52′58″ | 29°45′12″ |
| Kozakırmezarı | W of Kocakırmezarı Hill, on the road of Baklan Hill, Çaylak stream | MBG-4 | 38°53′12″ | 29°45′10″ |
| Kozakırmezarı | NW of Kocakırmezarı Hill, E of Çaylak stream | MBG-5 | 38°53′16″ | 29°45′10″ |
| Kozakırmezarı | W of Kocakırmezarı Hill, W of Çaylak stream | MBG-6 | 38°53′16″ | 29°45′03″ |
| Tepedelen | E of Tepedelen Hill, Tepedelen spring | MBG-7 | 38°54′23″ | 29°44′43″ |
| Pazarcık | Pazarcık ridge | MBG-8 | 38°53′12″ | 29°44′39″ |
| Pazarcık | W of Pazarcık ridge | MBG-9 | 38°53′09″ | 29°44′36″ |
| Baklan | E foothills of Baklan Hill | MBG-10 | 38°53′20″ | 29°43′42″ |
| Baklan | E of Baklan Hill, on the road of Baklan Hill | MBG-11 | 38°53′29″ | 29°43′00″ |
| Baklan | SE of Baklan Hill, on the road of Baklan Hill | MBG-12 | 38°53′24″ | 29°43′16″ |
| Baklan | Foothills of the Baklan Hill, on the road of the Tepedelen spring | MBGT-1 | 38°54′12″ | 29°44′20″ |
| Gürlek | Dede stream, E of Ballık ridge | MBGG-1 | 38°51′41″ | 29°42′45″ |
| Gürlek | Dede stream, E of Tömsü Hill | MBGA-1 | 38°51′20″ | 29°41′04″ |
| Göçyolu | W of Baklan Hill, Göçyolu, NW of Başçaylı Hill | MBGY-1 | 38°53′35″ | 29°43′05″ |
| Göçyolu | W of Baklan Hill, Göçyolu, NW of Başçaylı Hill | MBGY-2 | 38°53′36″ | 29°43′10″ |

Table 2
Petrographic features of the representative samples of Baklan Granite

| Location | Sample | Rock type[a] | Major phases | Accessories | Grain size | Texture |
|---|---|---|---|---|---|---|
| Kozakırmezarı | MBG-2 | Granodiorite | bio, hbl, pl, ksp, qz | op, ap | Medium coarse | Hypidiomorphic |
| Kozakırmezarı | MBG-3 | Granodiorite | bio, hbl, pl, ksp, qz | op, ap, ttn | Medium coarse | Hypidiomorphic |
| Kozakırmezarı | MBG-4 | Granodiorite | bio, hbl, pl, ksp, qz | op, ap, ttn | Medium coarse | Hypidiomorphic |
| Kozakırmezarı | MBG-5 | Granodiorite | bio, hbl, pl, ksp, qz | op, ap | Medium coarse | Hypidiomorphic |
| Kozakırmezarı | MBG-6 | Granodiorite | bio, hbl, pl, ksp, qz | op, ap, ttn | Medium coarse | Hypidiomorphic |
| Tepedelen | MBG-7 | Granodiorite | bio, hbl, pl, ksp, qz | op, ap, ttn | Medium coarse | Hypidiomorphic |
| Pazarcık | MBG-8 | Granodiorite | bio, hbl, pl, ksp, qz | op, ap, ttn | Medium coarse | Hypidiomorphic |
| Pazarcık | MBG-9 | Granodiorite | bio, hbl, pl, ksp, qz | op, ap, ttn | Medium coarse | Hypidiomorphic |
| Baklan | MBG-10 | Granodiorite | bio, hbl, pl, ksp, qz | op, ap, ttn | Medium coarse | Hypidiomorphic, porphyric |
| Baklan | MBG-11 | Granodiorite | bio, hbl, pl, ksp, qz | op, ap, ttn | Medium coarse | Hypidiomorphic |
| Baklan | MBG-12 | Granodiorite | bio, hbl, pl, ksp, qz | op, ap, ttn | Medium coarse | Hypidiomorphic |
| Baklan | MBGT-1 | Granodiorite | bio, hbl, pl, ksp, qz | op, ap, ttn | Medium coarse | Hypidiomorphic |
| Gürlek | MBGG-1 | Granodiorite | bio, hbl, pl, ksp, qz | op, ap, ttn | Medium coarse | Hypidiomorphic |
| Gürlek | MBGA-1 | Granodiorite | bio, hbl, pl, ksp, qz | op, ap, ttn | Medium coarse | Hypidiomorphic, graphic |
| Göçyolu | MBGY-1 | Granodiorite | bio, hbl, pl, ksp, qz | op, ap, ttn | Medium coarse | Hypidiomorphic |
| Göçyolu | MBGY-2 | Granodiorite | bio, hbl, pl, ksp, qz | op, ap, ttn | Medium coarse | Hypidiomorphic |

*Mineral abbreviations:* bio, biotite; hbl, hornblende; pl, plagioclase; ksp, K-feldspar; qz, quartz; op, opaque; ap, apatite; ttn, titanite.
[a] Rock type is taken from nomenclature of Debon and Le Fort (1983).

scanned geological map segments which can be obtained from the corresponding author upon request.

Following a preliminary microscopic examination, 26 samples were chosen for chemical analyses. All samples were analyzed at the Activation Laboratories Ltd. (Canada). Major oxides and trace element abundances were determined using Inductively Coupled Plasma Atomic Emission Spectrometry (ICP-AES) following a $LiBO_2$fusion

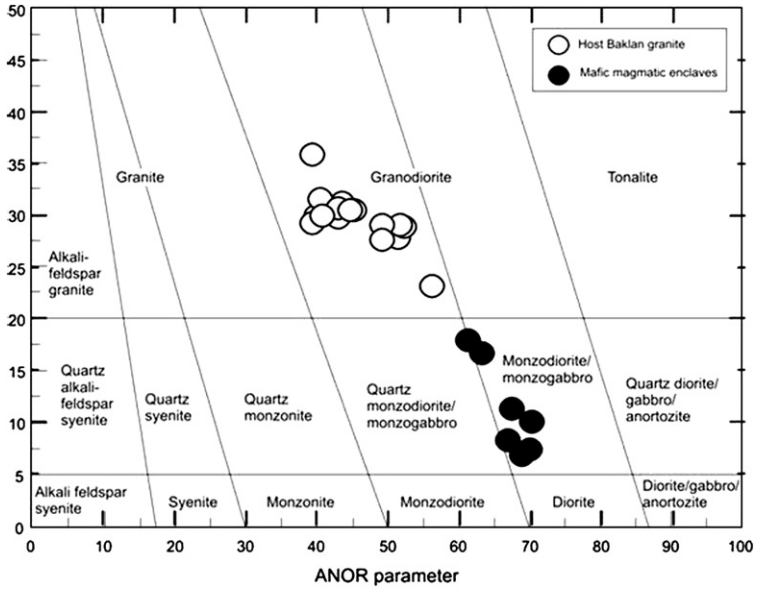


Fig. 4. Plot of $Q$ parameter vs. ANOR parameter (after Streckeisen and Le Maitre, 1979) used to classify the Baklan rocks and its mafic enclaves. [$Q$ parameter $= 100 \times Q/(Q + \mathrm{Or} + \mathrm{Ab} + \mathrm{An})$; [ANOR parameter $= 100 \times \mathrm{An}/(\mathrm{Or} + \mathrm{An})$]: *Note:* the norm calculations are made following the procedure reported by Cox et al. (1979).

Table 3
K–Ar ages for representative samples of Baklan Granite in southern part of the Muratdağı Region, western Turkey

| Sample number | Location | Rock type | Method | $K_2O$ (wt.%) | Radiogenic $^{40}Ar$ ($10^{-3}$ mm$^3$/g) | % Atmosphere | Age (Ma $\pm 1\sigma$) |
|---|---|---|---|---|---|---|---|
| MBG-6 | Kocakırmezarı | Granodiorite | Whole-rock | 2.63 | 1.795 | 68.3 | $17.8 \pm 0.7$ |
| MBG-8 | Pazarcık | Granodiorite | Whole-rock | 2.60 | 1.932 | 75.3 | $19.4 \pm 0.9$ |
| MBGT-1 | Baklan | Granodiorite | Whole-rock | 2.64 | 1.957 | 73.8 | $19.3 \pm 0.7$ |

Table 4
Major (wt.%) and trace (ppm) element compositions of mafic microgranular enclaves (mdr) and host Baklan Granodiorite (gdr)

| Sample number | MBG-2 | MBG-3 | MBG-4 | MBG-5 | MBG-6 | MBG-7 | MBG-8 | MBG-9 |
|---|---|---|---|---|---|---|---|---|
| Rock type | gdr | gdr | gdr | gdr | gdr | gdr | gdr | gdr |
| $SiO_2$ | 67.49 | 67.05 | 68.69 | 68.09 | 68.27 | 65.12 | 67.51 | 67.40 |
| $TiO_2$ | 0.38 | 0.40 | 0.42 | 0.40 | 0.40 | 0.50 | 0.40 | 0.41 |
| $Al_2O_3$ | 15.75 | 15.18 | 14.93 | 15.37 | 14.86 | 15.28 | 15.68 | 15.54 |
| $Fe_2O_{3tot}$ | 2.98 | 3.28 | 3.31 | 3.15 | 3.28 | 4.27 | 3.35 | 3.30 |
| MnO | 0.05 | 0.09 | 0.05 | 0.05 | 0.05 | 0.07 | 0.06 | 0.06 |
| MgO | 1.21 | 1.36 | 1.37 | 1.52 | 1.55 | 2.24 | 1.48 | 1.48 |
| CaO | 2.86 | 3.30 | 2.94 | 3.22 | 3.28 | 4.17 | 2.93 | 3.02 |
| $Na_2O$ | 3.24 | 2.83 | 3.08 | 3.12 | 2.96 | 2.75 | 3.14 | 3.05 |
| $K_2O$ | 3.60 | 3.58 | 3.61 | 3.59 | 3.65 | 3.10 | 3.80 | 3.70 |
| $P_2O_5$ | 0.13 | 0.13 | 0.12 | 0.12 | 0.11 | 0.12 | 0.13 | 0.14 |
| L.O.I. | 0.00 | 2.00 | 0.70 | 0.60 | 0.80 | 1.60 | 0.70 | 1.10 |
| Sum | 99.19 | 99.20 | 99.22 | 99.23 | 99.21 | 99.23 | 99.18 | 99.20 |
| Rb | 160.90 | 135.60 | 168.40 | 155.60 | 165.40 | 122.10 | 155.30 | 176.70 |
| Sr | 378.10 | 393.50 | 305.30 | 340.10 | 335.30 | 403.30 | 360.80 | 374.10 |
| Ba | 917.80 | 726.80 | 625.30 | 700.00 | 810.30 | 731.20 | 1035.00 | 884.10 |
| Zr | 166.70 | 159.00 | 149.30 | 127.60 | 132.60 | 138.20 | 155.00 | 159.50 |
| Hf | 5.20 | 4.60 | 4.80 | 4.10 | 4.20 | 4.40 | 4.70 | 4.80 |
| Ta | 1.40 | 1.60 | 1.70 | 1.40 | 1.70 | 1.90 | 1.50 | 1.80 |
| Th | 19.20 | 17.80 | 15.30 | 24.20 | 14.00 | 42.90 | 16.70 | 17.40 |
| U | 5.90 | 9.30 | 9.00 | 7.70 | 7.40 | 14.10 | 7.10 | 6.00 |
| Nb | 18.50 | 16.20 | 17.30 | 13.40 | 13.80 | 16.80 | 18.30 | 19.60 |
| Y | 19.50 | 21.90 | 21.00 | 17.90 | 17.40 | 26.20 | 19.90 | 23.40 |
| Cs | 3.70 | 2.10 | 5.10 | 3.50 | 3.60 | 2.60 | 3.30 | 7.20 |
| Ga | 21.00 | 19.20 | 19.00 | 19.30 | 19.80 | 18.60 | 19.40 | 20.60 |
| V | 42.00 | 56.00 | 57.00 | 60.00 | 68.00 | 89.00 | 51.00 | 53.00 |
| Cr | 7 | 7 | 7 | 13.7 | 21 | 21 | 7 | 7 |
| Ni | 5.70 | 7.40 | 10.20 | 8.30 | 9.00 | 8.90 | 8.00 | 6.30 |
| Co | 5.40 | 6.70 | 7.30 | 8.30 | 7.80 | 11.10 | 6.30 | 7.00 |
| Sc | 5.00 | 6.00 | 6.00 | 6.00 | 7.00 | 10.00 | 7.00 | 6.00 |
| La | 41.30 | 34.40 | 31.80 | 29.60 | 34.10 | 32.80 | 38.80 | 35.00 |
| Ce | 82.30 | 71.80 | 68.40 | 60.90 | 69.60 | 70.30 | 80.80 | 72.50 |
| Pr | 8.18 | 7.27 | 6.71 | 5.95 | 6.63 | 7.11 | 7.79 | 7.26 |
| Nd | 30.30 | 26.40 | 25.00 | 21.80 | 22.50 | 25.90 | 27.50 | 26.20 |
| Sm | 5.10 | 5.40 | 4.50 | 4.10 | 4.00 | 5.10 | 4.80 | 5.00 |
| Eu | 1.17 | 1.02 | 0.88 | 0.87 | 0.87 | 1.04 | 0.98 | 1.03 |
| Gd | 3.95 | 4.32 | 3.77 | 3.24 | 3.27 | 4.12 | 3.58 | 4.27 |
| Tb | 0.61 | 0.64 | 0.61 | 0.52 | 0.48 | 0.69 | 0.57 | 0.64 |
| Dy | 3.22 | 3.71 | 3.26 | 2.90 | 2.75 | 3.92 | 3.29 | 3.55 |
| Ho | 0.63 | 0.74 | 0.66 | 0.55 | 0.56 | 0.85 | 0.62 | 0.70 |
| Er | 1.71 | 1.98 | 2.00 | 1.66 | 1.58 | 2.43 | 1.94 | 2.04 |
| Tm | 0.25 | 0.31 | 0.30 | 0.26 | 0.24 | 0.37 | 0.27 | 0.30 |
| Yb | 1.76 | 2.01 | 2.08 | 1.80 | 1.72 | 2.46 | 1.83 | 2.02 |
| Lu | 0.27 | 0.28 | 0.32 | 0.27 | 0.26 | 0.39 | 0.33 | 0.33 |

| Sample number | MBG-10 | MBG-11 | MBG-12 | MBGT-1 | MBGG-1 | MBGA-1 | MBGY-1 | MBGY-2 | BGTA-1 | BMGE-1 | BMGE-2 |
|---|---|---|---|---|---|---|---|---|---|---|---|
| Rock type | gdr | gdr | gdr | gdr | gdr | gdr | gdr | gdr | mdr | mdr | mdr |
| $SiO_2$ | 65.60 | 62.47 | 66.75 | 64.99 | 65.89 | 65.57 | 70.94 | 67.53 | 53.55 | 53.93 | 54.74 |
| $TiO_2$ | 0.48 | 0.60 | 0.51 | 0.56 | 0.50 | 0.53 | 0.35 | 0.47 | 0.98 | 1.00 | 0.87 |
| $Al_2O_3$ | 15.54 | 16.49 | 14.76 | 15.10 | 15.13 | 15.05 | 13.70 | 14.71 | 17.11 | 17.07 | 15.65 |
| $Fe_2O_{3tot}$ | 4.20 | 4.95 | 4.10 | 4.74 | 4.37 | 4.49 | 2.70 | 3.91 | 8.74 | 8.85 | 7.98 |
| MnO | 0.07 | 0.08 | 0.06 | 0.08 | 0.07 | 0.06 | 0.05 | 0.07 | 0.18 | 0.17 | 0.2 |
| MgO | 2.14 | 2.54 | 2.02 | 2.41 | 2.19 | 2.21 | 1.31 | 2.01 | 4.85 | 4.91 | 6.32 |
| CaO | 4.16 | 4.95 | 3.65 | 4.19 | 4.18 | 3.91 | 2.95 | 3.49 | 6.86 | 6.69 | 7.21 |
| $Na_2O$ | 2.98 | 2.96 | 2.61 | 2.88 | 2.93 | 2.78 | 2.68 | 2.83 | 3.85 | 3.83 | 3.37 |
| $K_2O$ | 3.14 | 3.01 | 3.63 | 3.25 | 3.03 | 3.28 | 3.73 | 3.55 | 2.07 | 1.84 | 1.63 |
| $P_2O_5$ | 0.12 | 0.15 | 0.13 | 0.14 | 0.13 | 0.15 | 0.08 | 0.12 | 0.21 | 0.21 | 0.17 |
| L.O.I. | 0.80 | 0.90 | 1.00 | 0.90 | 0.80 | 1.20 | 0.70 | 0.40 | 0.005 | 0.006 | 0.045 |
| Sum | 99.23 | 99.11 | 99.22 | 99.25 | 99.22 | 99.23 | 99.19 | 99.09 | 98.405 | 98.506 | 98.185 |
| Rb | 136.00 | 116.50 | 150.40 | 129.60 | 119.50 | 141.30 | 143.20 | 136.80 | 110.9 | 108.5 | 76.7 |

Table 4 (*continued*)

| Sample number | MBG-10 | MBG-11 | MBG-12 | MBGT-1 | MBGG-1 | MBGA-1 | MBGY-1 | MBGY-2 | BGTA-1 | BMGE-1 | BMGE-2 |
|---|---|---|---|---|---|---|---|---|---|---|---|
| Rock type | gdr | gdr | gdr | gdr | gdr | gdr | gdr | gdr | mdr | mdr | mdr |
| Sr | 436.70 | 453.80 | 388.70 | 393.40 | 394.30 | 365.10 | 280.70 | 294.00 | 337.2 | 330.6 | 332.0 |
| Ba | 792.40 | 855.90 | 888.60 | 734.10 | 761.40 | 748.00 | 680.60 | 637.50 | 533.3 | 474.3 | 434.8 |
| Zr | 137.90 | 148.80 | 137.90 | 149.80 | 132.60 | 155.30 | 101.60 | 102.20 | 154.6 | 143.1 | 170.5 |
| Hf | 4.40 | 4.30 | 4.30 | 4.50 | 4.10 | 5.00 | 3.30 | 3.50 | 4.8 | 4.8 | 5.5 |
| Ta | 1.10 | 1.10 | 1.90 | 1.40 | 1.20 | 1.60 | 1.70 | 1.30 | 2.4 | 2.0 | 1.1 |
| Th | 10.80 | 12.70 | 14.40 | 11.40 | 17.50 | 15.70 | 33.20 | 18.30 | 11.6 | 13.9 | 5.7 |
| U | 4.10 | 4.00 | 4.90 | 4.10 | 7.60 | 6.50 | 6.80 | 7.20 | 8.6 | 8.4 | 5.8 |
| Nb | 12.70 | 13.50 | 16.60 | 14.40 | 12.60 | 15.20 | 13.80 | 13.30 | 25 | 21.5 | 17.0 |
| Y | 19.60 | 22.10 | 27.40 | 23.00 | 20.90 | 22.90 | 20.80 | 18.70 | 45.5 | 38.9 | 39.6 |
| Cs | 3.80 | 2.10 | 4.20 | 3.50 | 3.20 | 5.10 | 5.00 | 5.70 | 6 | 5.5 | 2.1 |
| Ga | 20.10 | 18.70 | 18.50 | 18.60 | 17.40 | 18.90 | 14.70 | 15.70 | 23.5 | 22.0 | 20.2 |
| V | 91.00 | 102.00 | 84.00 | 105.00 | 91.00 | 90.00 | 52.00 | 73.00 | 223 | 217.0 | 156.0 |
| Cr | 21.00 | 21.00 | 14.00 | 27.00 | 14.00 | 21.00 | 7.00 | 14.00 | 34 | 41.0 | 308.0 |
| Ni | 6.80 | 9.30 | 9.20 | 8.30 | 7.80 | 10.70 | 5.10 | 8.70 | 9.9 | 18.0 | 69.0 |
| Co | 12.30 | 13.90 | 10.70 | 13.50 | 11.90 | 11.20 | 6.20 | 9.50 | 23.7 | 23.0 | 23.7 |
| Sc | 9.00 | 11.00 | 9.00 | 10.00 | 10.00 | 9.00 | 6.00 | 8.00 | 27 | 27.0 | 28.0 |
| La | 24.40 | 27.10 | 33.10 | 26.50 | 32.90 | 28.10 | 73.00 | 26.10 | 36.6 | 32.2 | 23.1 |
| Ce | 51.40 | 61.30 | 75.60 | 60.30 | 67.70 | 61.80 | 131.50 | 55.60 | 101.3 | 88.8 | 63.6 |
| Pr | 5.33 | 6.40 | 7.92 | 6.39 | 6.56 | 6.48 | 10.72 | 5.45 | 10.89 | 9.47 | 7.39 |
| Nd | 19.50 | 23.90 | 29.60 | 24.60 | 23.30 | 25.80 | 31.70 | 20.80 | 40.2 | 34.8 | 29.8 |
| Sm | 3.60 | 4.60 | 6.00 | 4.70 | 4.40 | 4.80 | 4.70 | 3.80 | 8.7 | 7.6 | 7.2 |
| Eu | 0.97 | 1.10 | 1.19 | 1.01 | 1.01 | 1.05 | 0.87 | 0.81 | 1.58 | 1.44 | 1.47 |
| Gd | 3.18 | 3.79 | 5.14 | 3.94 | 3.48 | 4.36 | 3.30 | 3.22 | 7.55 | 6.81 | 6.64 |
| Tb | 0.53 | 0.64 | 0.81 | 0.63 | 0.55 | 0.64 | 0.54 | 0.53 | 1.28 | 1.15 | 1.09 |
| Dy | 3.29 | 3.49 | 4.60 | 3.71 | 3.23 | 3.79 | 3.12 | 2.96 | 7.02 | 6.05 | 6.2 |
| Ho | 0.63 | 0.70 | 0.90 | 0.76 | 0.70 | 0.76 | 0.66 | 0.62 | 1.41 | 1.2 | 1.25 |
| Er | 1.77 | 2.08 | 2.51 | 2.13 | 2.04 | 2.16 | 1.99 | 1.83 | 4.78 | 3.86 | 3.97 |
| Tm | 0.28 | 0.33 | 0.37 | 0.38 | 0.32 | 0.33 | 0.32 | 0.30 | 0.69 | 0.6 | 0.59 |
| Yb | 1.93 | 2.10 | 2.48 | 2.27 | 2.10 | 2.18 | 2.11 | 2.01 | 4.35 | 3.66 | 3.74 |
| Lu | 0.29 | 0.33 | 0.36 | 0.35 | 0.33 | 0.32 | 0.31 | 0.31 | 0.67 | 0.61 | 0.61 |

| Sample number | BMGE-3 | BMGE-4 | BMGE-5 | BMGE-6 | BMGE-7 | BMGE-8 | BMGY-1 |
|---|---|---|---|---|---|---|---|
| Rock type | mdr | mdr | mdr | mdr | mdr | mdr | mdr |
| $SiO_2$ | 54.6 | 58.79 | 58.83 | 58.39 | 55.45 | 54.4 | 55.38 |
| $TiO_2$ | 0.93 | 0.72 | 0.73 | 0.76 | 0.90 | 1.16 | 1.03 |
| $Al_2O_3$ | 17.14 | 13.28 | 15.34 | 15.49 | 16.08 | 17.96 | 15.95 |
| $Fe_2O_{3tot}$ | 8.14 | 7.88 | 6.87 | 7.1 | 7.47 | 8.36 | 8.18 |
| MnO | 0.17 | 0.21 | 0.16 | 0.16 | 0.19 | 0.13 | 0.2 |
| MgO | 4.75 | 6.1 | 4.63 | 4.69 | 5.6 | 4.11 | 4.83 |
| CaO | 7.14 | 7.47 | 6.59 | 6.76 | 7.24 | 5.88 | 5.79 |
| $Na_2O$ | 3.87 | 2.8 | 3.17 | 3.31 | 3.78 | 3.97 | 3.9 |
| $K_2O$ | 1.77 | 1.18 | 2.24 | 2.1 | 1.81 | 2.4 | 1.72 |
| $P_2O_5$ | 0.18 | 0.16 | 0.13 | 0.14 | 0.18 | 0.28 | 0.21 |
| L.O.I. | 0.004 | 0.04 | 0.01 | 0.01 | 0.022 | 0.003 | 0.007 |
| Sum | 98.694 | 98.63 | 98.7 | 98.91 | 98.722 | 98.653 | 97.197 |
| Rb | 84.6 | 40.2 | 78.7 | 70.4 | 86.8 | 133.9 | 117.5 |
| Sr | 406.7 | 307.6 | 347.3 | 339.1 | 279.2 | 408.1 | 261.6 |
| Ba | 485.1 | 211.1 | 371.3 | 342.8 | 346.4 | 711.1 | 557.3 |
| Zr | 137.8 | 112 | 201.8 | 176.3 | 145.5 | 229.3 | 155.4 |
| Hf | 4.8 | 3.6 | 5.9 | 5.7 | 4.7 | 5.9 | 5.2 |
| Ta | 1.6 | 1.3 | 1.2 | 1.4 | 2.0 | 1.5 | 3.4 |
| Th | 10.9 | 5.5 | 9 | 10.2 | 7.6 | 9.2 | 8.6 |
| U | 5.1 | 4.1 | 4.3 | 5 | 5.8 | 7.2 | 13 |
| Nb | 16.3 | 21.6 | 15 | 15.3 | 20.9 | 18.5 | 30.3 |
| Y | 31.9 | 88.4 | 38.6 | 38.4 | 40.1 | 24.1 | 42.1 |
| Cs | 3.5 | 1 | 1.5 | 1.2 | 3.2 | 4.1 | 4.4 |
| Ga | 19.2 | 18.2 | 18 | 18.3 | 19.2 | 22.8 | 22.4 |
| V | 200 | 153 | 153 | 152 | 162 | 177 | 170 |
| Cr | 27 | 274 | 68 | 68 | 151 | 21 | 48 |
| Ni | 25 | 48 | 32 | 29 | 33 | 18 | 29 |
| Co | 22.9 | 25.2 | 19.7 | 19.2 | 22.9 | 22.2 | 21.5 |
| Sc | 22 | 40 | 27 | 28 | 25 | 17 | 25 |

(*continued on next page*)

Table 4 (*continued*)

| Sample number<br>Rock type | BMGE-3<br>mdr | BMGE-4<br>mdr | BMGE-5<br>mdr | BMGE-6<br>mdr | BMGE-7<br>mdr | BMGE-8<br>mdr | BMGY-1<br>mdr |
|---|---|---|---|---|---|---|---|
| La | 36.5 | 42.1 | 27.9 | 28.4 | 37.6 | 38.7 | 38.3 |
| Ce | 91.5 | 117.7 | 74.9 | 79.2 | 102.5 | 83.3 | 105 |
| Pr | 8.81 | 13.89 | 8.57 | 8.72 | 10.73 | 7.53 | 10.52 |
| Nd | 30.5 | 59.6 | 33.8 | 32.1 | 39.7 | 27 | 36.4 |
| Sm | 6.2 | 14.2 | 7.5 | 7.7 | 8.6 | 5.5 | 7.2 |
| Eu | 1.52 | 1.88 | 1.45 | 1.41 | 1.5 | 1.06 | 1.14 |
| Gd | 5.32 | 14.85 | 6.87 | 6.22 | 6.97 | 4.24 | 6.31 |
| Tb | 0.91 | 2.56 | 1.13 | 1.11 | 1.23 | 0.76 | 1.05 |
| Dy | 5.14 | 14.73 | 6.16 | 6.19 | 6.99 | 3.75 | 6.2 |
| Ho | 1.01 | 2.95 | 1.24 | 1.18 | 1.3 | 0.78 | 1.19 |
| Er | 3.13 | 8.84 | 3.8 | 3.91 | 4.07 | 2.28 | 4.15 |
| Tm | 0.52 | 1.3 | 0.6 | 0.61 | 0.68 | 0.38 | 0.67 |
| Yb | 3.09 | 7.75 | 3.79 | 3.81 | 4.02 | 2.27 | 4.28 |
| Lu | 0.51 | 1.15 | 0.63 | 0.63 | 0.69 | 0.4 | 0.7 |

Major oxides and trace element abundances were determined using ICP-AES, and REE contents were measured by ICP-MS at Actlab in Canada.

and dilute nitric acid digestion. Rare earth element (REE) contents were measured by Inductively Coupled Plasma Atomic Mass Spectrometry (ICP-MS). Loss on ignition (LOI) is by weight difference after ignition at 1000 °C.

K–Ar age determinations of three fresh samples were carried out at the Actlabs in Canada. The K concentration was measured by ICP. The argon analysis was conducted using the isotope dilution procedure on noble gas mass spectrometry. Aliquot of the sample was weighed into Al container, loaded into sample system of extraction unit, degassed at ~100 °C during 2 days to remove the surface gases. Argon was extracted from the sample in double vacuum furnace at 1700 °C. Argon concentration was determined using isotope dilution with $^{38}Ar$ spike, which was introduced to the sample system prior to each extraction. The extracted gases were cleaned up in two step purification system. Then pure Ar was introduced into a customer build magnetic sector mass spectrometer (Reinolds type) with Varian CH5 magnet. The ion source has an axial design (Baur–Signer source), which provide more than 90% transmission and extremely small isotopic mass-discrimination. Measurement of Ar isotope ratios was corrected for mass-discrimination and then atmospheric argon was removed assuming that $^{36}Ar$ is only from the air. Concentration of $^{40}Ar$ radiogenic was calculated by using $^{38}Ar$ spike concentration. After each analysis the extraction temperature was elevated to 1800 °C for few minutes and furnace was prepared for next analysis.

Radiogenic isotopes (Nd–Sr) were analyzed at the Actlabs in Canada. Rock powder was dissolved in a mixture of HF, $HNO_3$ and $HClO_4$. Before the decomposition samples were spiked with $^{149}Sm$–$^{150}Nd$ mixed spike solution. REE were separated on a BioRad AG1-X8 200–400 mesh resin using the conventional cation-exchange techniques. Sm and Nd were separated by extraction chromatography on LN-Spec (100–150 mesh) resin. Total blanks in the laboratory are 0.1–0.2 ng for Sm and 0.1–0.5 ng for Nd. Rb, Sr, Sm and Nd concentrations were measured 166 using isotopic dilution. Isotopic compositions of Sm and Nd were determined on a Triton TI 7-collector mass-spectrometer. Accuracy of the measurements of Sm and Nd contents were ±0.5%, $^{147}Sm/^{144}Nd$ – ±0.5%, $^{143}Nd/^{144}Nd$ – ±0.005% ($2\sigma$). $^{143}Nd/^{144}Nd$ ratios are given relative to the value of 0.511860 for the La Jolla standard. During the period of work the weighted average of five La Jolla Nd-standard runs yielded $0.511843 \pm 5$ ($2\sigma$) for $^{143}Nd/^{144}Nd$, using 0.7219 for $^{146}Nd/^{144}Nd$ to normalize. The results for the means of four runs of BCR-1 standard were 6.50 ppm Sm, 28.5 ppm Nd, $^{147}Sm/^{144}Nd = 0.1380$, $^{143}Nd/^{144}Nd = 0.512635 \pm 7$. Rock powders for Rb–Sr analysis were dissolved in a mixture of HF, $HNO_3$ and $HClO_4$. Before the decomposition all samples were totally spiked with $^{85}Rb$–$^{84}Sr$ mixed solution. Rb and Sr were separated using conventional cation-exchange techniques. Total blanks are 0.01–0.05 ng for Rb and 0.3–0.7 ng for Sr. Accuracy of the measurements of Rb, Sr contents –

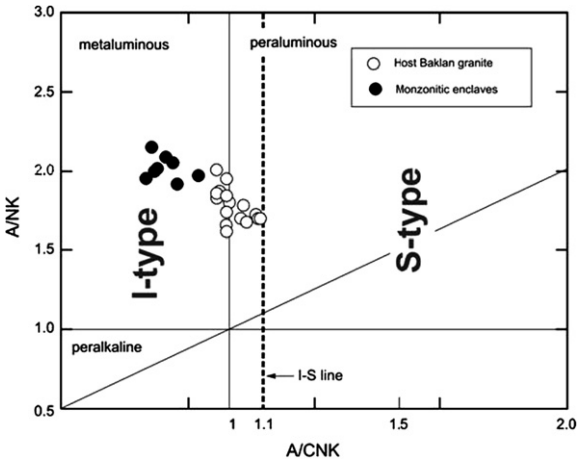


Fig. 5. The Shand's index diagram [A/CNK (molar ratio $Al_2O_3/(CaO + Na_2O + K_2O)$), A/NK (molar ratio $Al_2O_3/(Na_2O + K_2O)$)] for Baklan Granite and mafic enclaves (Shand, 1927). Discrimination fields for different types (e.g. I-type and S-type) of granitoid rocks (Maniar and Piccoli, 1989).

±0.5%, $^{87}Rb/^{86}Sr$ – 1.0%, $^{87}Sr^{86}Sr$ – 0.007% (2$\sigma$). During the period of work the weighted average of 15 SRM-987 Sr-standard runs yielded 0.71024 ± 2 (2s) for $^{87}Sr/^{86}Sr$. Sr isotopic ratios were normalized to $^{88}Sr/^{86}Sr = 8.37521$.

## 4. Petrography

The Baklan Granite commonly displays a spectacular exfoliation structure. The granitic rocks are classified as granodiorite. Petrographically, most Baklan rocks are leucocratic biotite- and hornblende-bearing granites, which are dominantly medium- to coarse-grained, displaying commonly and typically hypidiomorphic to weakly allotriomorphic texture. Plagioclase (oligoclase-andesine), K-feldspar (orthoclase), quartz, biotite and hornblende are major phases occurring in variable proportions. Apatite, titanite and opaques (e.g. magnetite) are ubiquitous accessory phases. Quartz generally occurs as anhedral crystals with irregular distorted boundaries and occupies the spaces between feldspars. Plagioclase displaying polysynthetic-twinning is hypidiomorphic and usually fine to medium-grained, euhedral. Some grains are well-zoned. K-feldspar phenocryst showing carlsbad twinning presents as medium-grained. It strongly exhibits a microperthitic to perthitic textures. In some cases, K-feldspar shows microcline twinning. Biotite occurs as medium to coarse-grained, partly altered to chlorite and contains inclusions of plagioclase and opaque mineral. It presents as prismatic crystals showing pale green to brown pleochroism. Slight to moderate alteration to chlorite in most samples is common. Amphibole is typical of hornblende and found as anhedral to euhedral forms. It is dark to palish green in color and underwent partial alteration to chlorite. Biotite and hornblende form schlieren textures. Zircon, clinopyroxene and epidote are sporadically observed. Epidote (particularly zoisite) occurs as veinlets within some granitic rocks. The textural relationships suggest that biotite crystallized first, followed by plagioclase and K-feldspar, and finally quartz. All samples contain hornblende, biotite, titanite and magnetite. Based on the criteria of Chappell and White (1974, 1992), these minerals are characteristics of I-type and based on the oxidation state, they are of the magnetite-series granitoids (Ishihara, 1977). Table 2 summarizes petrographic descriptions of the samples. In addition, the northern margin of the Baklan pluton (Fig. 3a and b) also includes abundant light-color aplitic dykes.

Mafic microgranular enclaves (Didier and Barbarin, 1991) have been commonly observed in the sharp contacts of the Baklan intrusion. They are classified as monzodiorite and monzogabro in composition (see Fig. 4). They have mostly fine-grained, equigranular, hypidiomorphic texture. The main minerals in the enclaves are amphibole, biotite, clinopyroxene, zoned K-feldspar, plagioclase, quartz with accessory apatite and zircon. Interaction (or hybridization) between mafic enclave and surrounding granitic magma is observed from the gradational contacts between them, suggesting that magma mixing/mingling occurred.

## 5. Geochronology

The cooling and emplacement ages of the Baklan intrusion are still debated. Previous K–Ar age determination

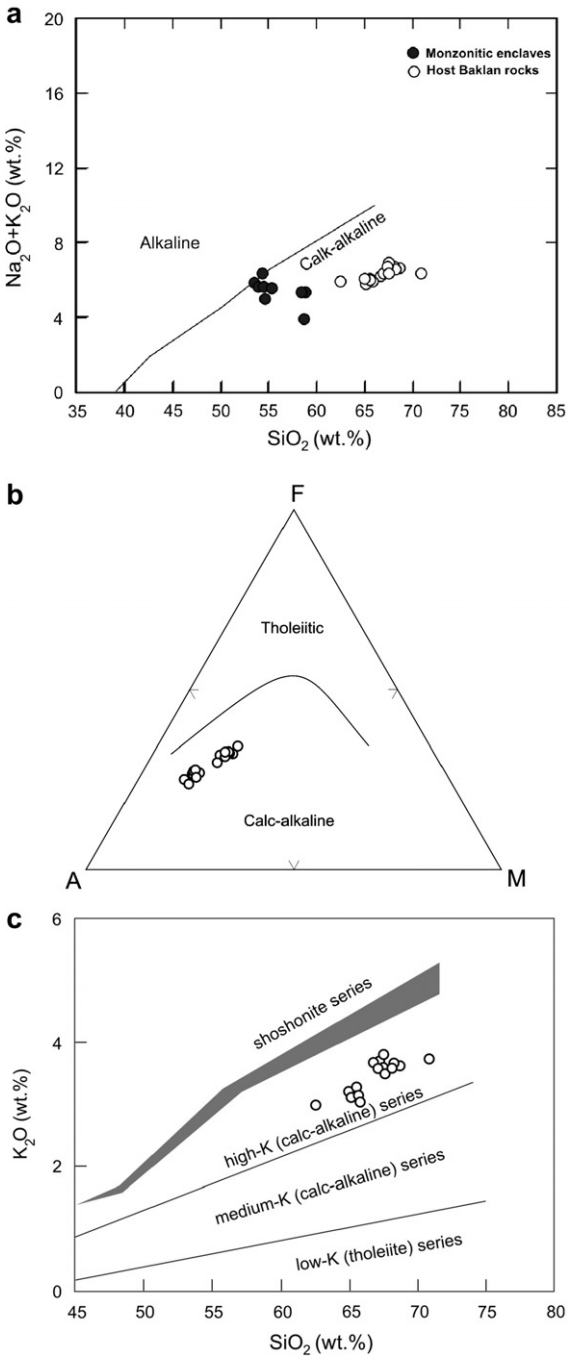


Fig. 6. Geochemical typology of the investigated Baklan Granite. (a) TAS diagram [(wt.% $Na_2O + K_2O$) vs. $SiO_2$] (divisions after Rickwood, 1989). Monzonitic enclaves are also plotted. (b) AFM diagram showing the boundary between the tholeiite and the calc-alkaline series of Irvine and Baragar (1971). A, F, M: weight percentage of total alkali ($Na_2O + K_2O$), total iron as FeO and MgO, respectively. (c) Plot of $K_2O$ vs. $SiO_2$ diagram showing the high-K calc-alkaline nature of the Baklan Granite (divisions after Rickwood, 1989).

gave $35.5 \pm 3.0$ Ma (Bingöl et al., 1982). In this work, samples collected from three different locations in the Baklan Granite were dated by the K–Ar method on the whole-rock, yielded ages between $17.8 \pm 0.7$ and $19.4 \pm 0.9$ Ma, which are very different from the published data (Table 3).

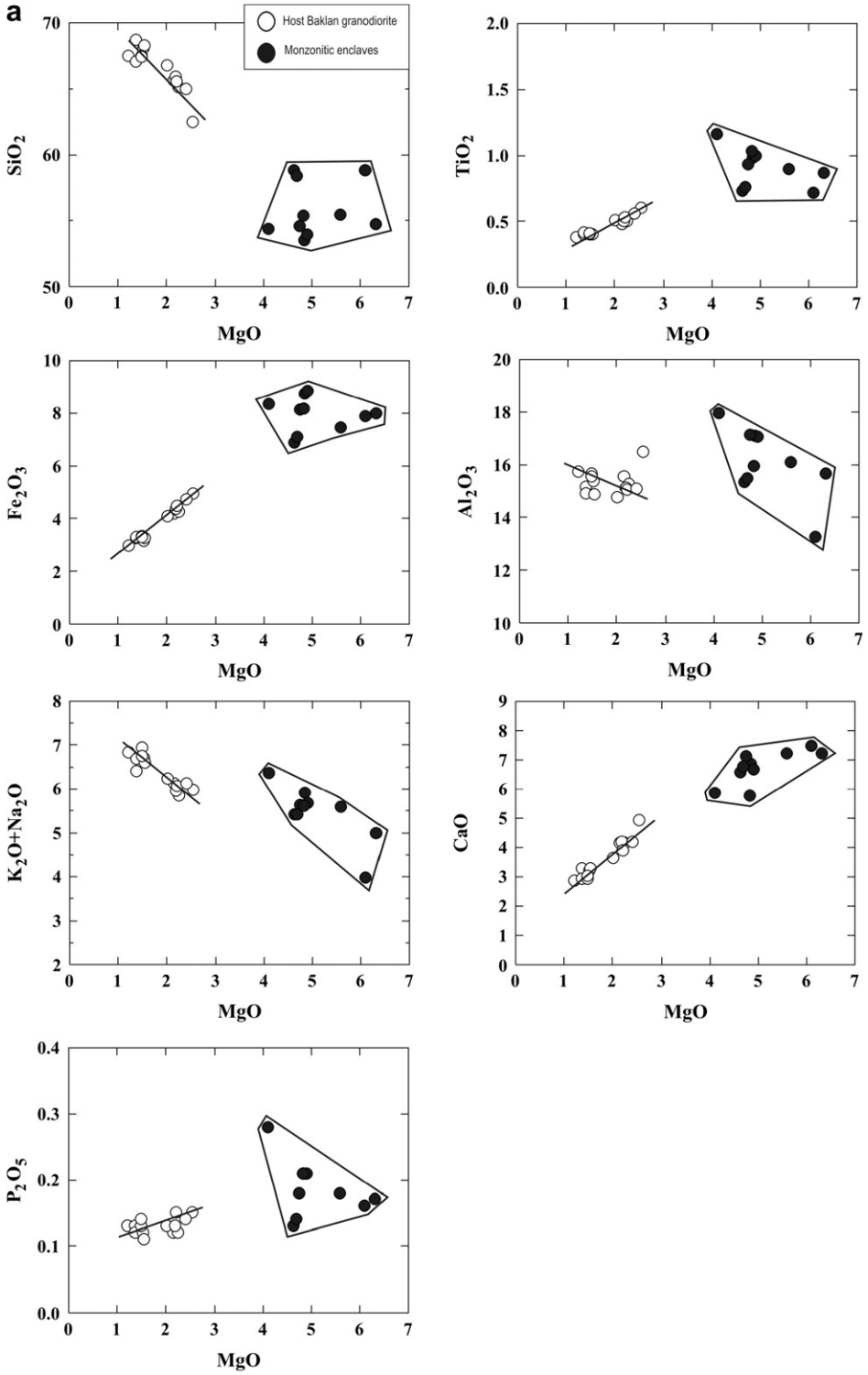


Fig. 7. (a) Various oxide plots [$SiO_2$, $TiO_2$, $Fe_2O_3$, $Al_2O_3$, $K_2O + Na_2O$, CaO, $P_2O_5$ vs. MgO (all expressed in wt.%)] and (b) trace element plots [Ni, Cr, La/Yb, Rb/Sr and Yb/Hf (all expressed in ppm)] vs. MgO variation diagrams for mafic enclaves and host rocks from Baklan Granite. Linear lines indicate evolutionary trends for the Baklan Granite.

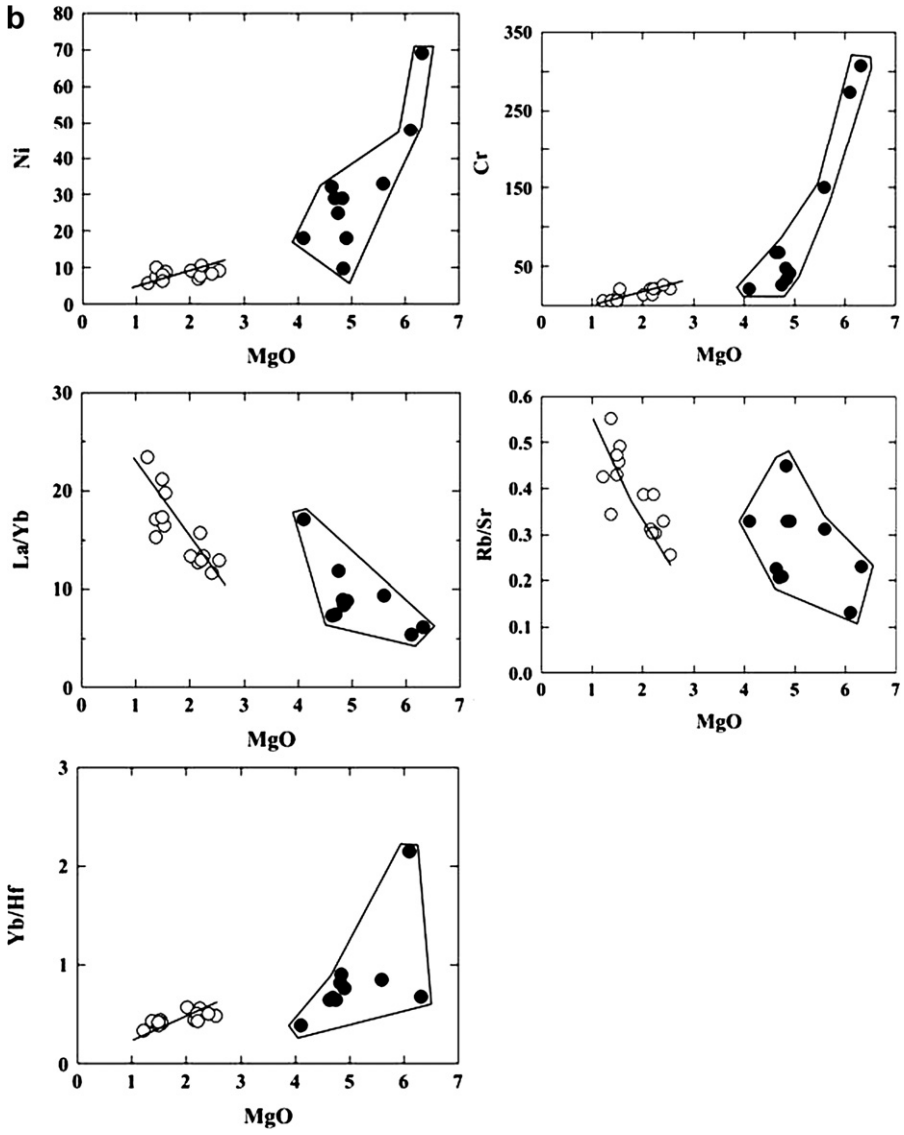


Fig. 7 (*continued*)

## 6. Results

### 6.1. Geochemistry

#### 6.1.1. Major and trace element compositions

The chemical compositions of the Baklan Granite and its enclaves are given in Table 4. The classification schemes of Streckeisen and Le Maitre (1979) confirm that Baklan Granite has granodioritic composition according to the normative mineralogy in *Q* parameter vs. ANOR parameter (Fig. 4). Shand's index [A/NK (molar $Al_2O_3/(Na_2O + K_2O)$) vs. A/CNK (molar $Al_2O_3/(Ca_2O + Na_2O + K_2O)$, Maniar and Piccoli, 1989)] defines these rocks as metaluminous to slightly peraluminous, and of I-type affinity (Fig. 5). In TAS and AFM diagrams (Fig. 6a and b), the samples plot in the sub-alkaline and calc-alkaline fields. Using the $K_2O$ vs. $SiO_2$ nomenclature of Rickwood (1989) all rocks plot within the high-K calc-alkaline field (Fig. 6c). Mafic enclaves are mafic to intermediate in composition ($SiO_2$ 53–59 wt.%, Table 4), and defined as monzogabro and monzodiorites (Fig. 4). They are metaluminous (A/CNK, 0.7–0.9), and calc-alkaline – slightly alkaline in character (Fig. 6a).

All Baklan samples are high in $SiO_2$ ranging from 62 to 71 wt.%. Mafic enclaves are rich in Cr (20–310 ppm), Ni (10–70 ppm) and Mg# (50–61) values (Table 4). In variation diagrams between major elements and MgO, the Baklan rocks commonly define a single linear trend for $SiO_2$, $TiO_2$, CaO, Cr, $Na_2O + K_2O$, $P_2O_5$, Rb/Sr, Yb/Hf, La/Yb, Cr and Ni, while enclaves plot in distinct fields (Fig. 7a and b).

Increasing $K_2O$ and Rb contents of host Baklan rocks, and decreasing $TiO_2$, $Fe_2O_3$, CaO and $Al_2O_3$ contents with decreasing MgO are compatible with the evolution through fractional crystallization processes (Fig. 7a and Table 4). Decreasing $TiO_2$ and $P_2O_5$ with decreasing MgO content are attributed to fractionation of titanite and apatite, respectively. Fractionation of plagioclase and K-feldspar

has also played important role on the petrogenesis of the Baklan Granite, as suggested by negative anomalies of Eu, Ba and Sr (Figs. 8a and 9). That is also confirmed with the small, but significant negative Eu anomaly (expressed as $Eu/Eu^*$) which increases with decreasing Sr, indicating the role of plagioclases during fractional crystallization (Fig. 10a). Fractional crystallization is also supported by the striking depletions in P and Ti, shown in the spidergrams (Fig. 9). Negative Ti anomalies are considered to be related to fractionation of Ti-bearing phases (ilmenite, titanite) and negative P anomalies result from apatite separation. The fractionation of accessory phases, i.e. zircon and titanite, can account for depletion in Zr and Y. It appears that crystal fractionation has played a significant role during the formation of the Baklan Granite. Fractionation relationships between LREE and HREE can also be helpful in monitoring fractional crystallization prosess (e.g. Jung et al., 2002). In the $(Ce/Yb)_N$ and $Yb_N$ vs. $TiO_2$ (wt.%) plot (Fig. 10c and d), the $(Ce/Yb)_N$ ratio increases and the $Yb_N$ content decreases with decreasing $TiO_2$, indicating modification of the $Ce/Yb_N$ ratio and the $Yb_N$ concentration during fractional crystallization.

Enrichment of LREE, together with depletion of HREE during fractional crystallization, is compatible with fractionation of amphibole, trending to concentrate the HREE. These observations on the Baklan Granite chemistry may be attributed to the derivation from the partial melting of a mafic source with plagioclase and/or amphibole as residue (Fig. 10b). The Baklan samples having low initial $^{87}Sr/^{86}Sr$ ratios include high Rb/Sr ratios (0.26–0.51), which are usually attributed to the partial melting processes involving mica breakdown and/or late plagioclase fractionation. Kemp and Hawkesworth (2003) point out that the Rb/Sr ratios of granitoids can reflect

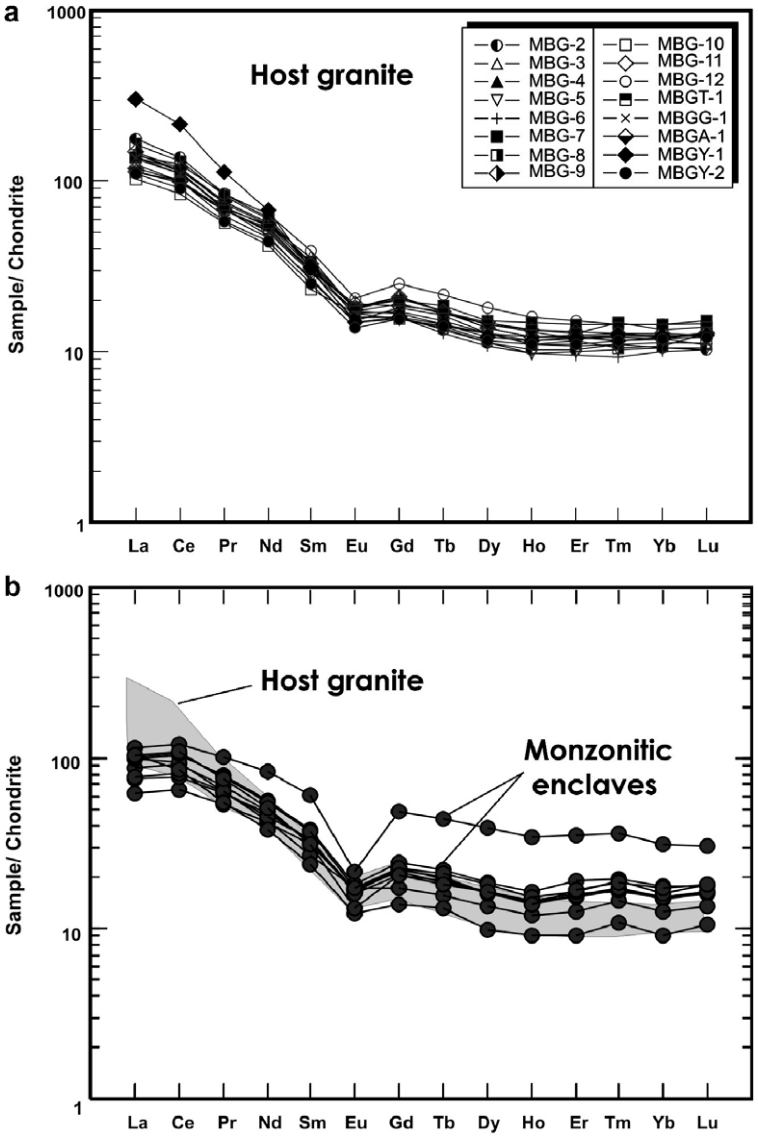


Fig. 8. Chondrite-normalized REE abundance patterns (normalized to values given by Sun and McDonough, 1989) for representative samples from Baklan Granite (a) and monzonitic enclaves (b).

the Rb/Sr ratios of their source rocks. Hence, the source of Baklan rocks would have high Rb/Sr ratios, but low initial $^{87}Sr/^{86}Sr$ ratios, may be indicative of a mica-bearing source.

The Baklan rocks have plot in low $Al_2O_3/(FeO_{tot} + MgO + TiO_2)$, $(Na_2O + K_2O)/(FeO_{tot} + MgO + TiO_2)$ fields in Fig. 11a and b and have a rather high and narrow range of $CaO/(FeO_{tot} + MgO + TiO_2)$ ratios in Fig. 11c, indicate the originating from partial melting of mafic crustal source rocks (Patīno Douce, 1999).

They also display consistency with post-collisional granitoids fields in Rb vs. Y + Nb, Rb/Zr vs. $SiO_2$, and Rb–Hf–Ta variation diagrams (Pearce et al., 1984; Harris et al., 1986; Pearce, 1996) (Fig. 12a, b and c).

Chondrite-normalized REE patterns of all Baklan samples (Fig. 8a) are characterized by enrichment in light rare earth elements, with $[(La/Yb)_N = 9–17]$, and slightly negative Eu anomalies ($Eu/Eu^* = 0.62–0.86$). The REE patterns for the enclaves are marked by somewhat different enrichment in LREEs, variable negative Eu anomalies (Fig. 8b). The Eu anomaly for one sample (BMGE-4) with high MgO (6 wt.%), $SiO_2$ (58 wt.%) and HREE, is quite distinct (Fig. 8b), which show similarity with of some A-type granites (e.g. Yang et al., 2006). Enclaves have higher total REE contents (157–303 ppm) than the host granites (124–180 ppm, except for one sample-BMGY-1, 264 ppm), relatively (Table 4), indicating a REE-enriched source(s) on their genesis. Accordingly, similarities in REE patterns between host rocks and enclaves also may imply the existence of inner genetic relations.

The primitive mantle-normalized spidergrams show enrichment in large-ione-lithophile (LIL) (e.g. Cs, Rb, K), some high field strength (HFS) elements (e.g. Th, U), together with La and Ce, and distinct negative anomalies of Nb and Ti (Fig. 9a). The enclave samples in the primitive mantle-normalized variation diagram (Fig. 9b), most show

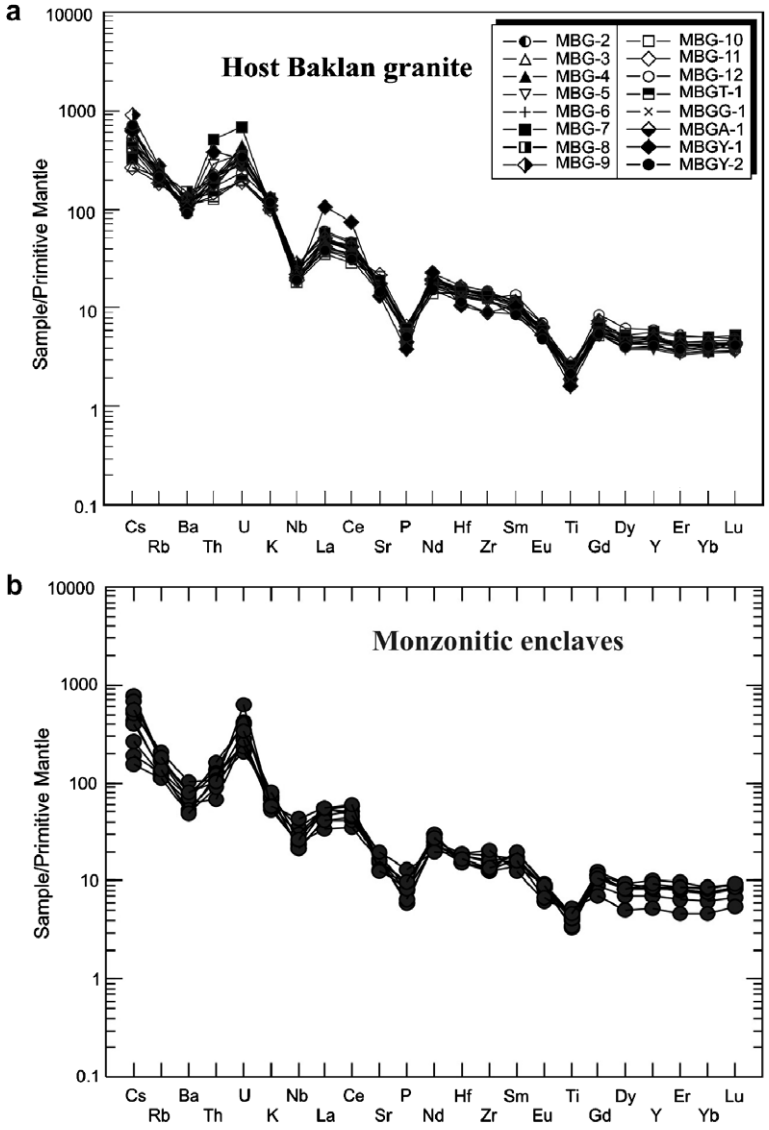


Fig. 9. Primitive mantle-normalized trace element abundances for representative samples from Baklan Granite and monzonitic enclaves. The normalizing values are from Sun and McDonough (1989).

the characteristic negative anomalies in Ba, Nb, P and Ti, together with the significant enrichment of U.

#### 6.1.2. Nd and Sr isotopic compositions

Rb, Sr, Sm and Nd concentrations and $^{143}Nd/^{144}Nd$ and $^{87}Sr/^{86}Sr$ ratios are listed in Table 5. The initial $^{87}Sr/^{86}Sr$ ratios and $\varepsilon_{Nd(t)}$ values have been calculated for ages of 19 Ma on the basis of whole-rock K–Ar dating. The data are shown in a plots of $(^{87}Sr/^{86}Sr)_i$ vs. $SiO_2$ and $\varepsilon_{Nd(t)}$ vs. $(^{87}Sr/^{86}Sr)_i$ (Fig. 13a and b). The Baklan Granite is characterized by low initial $^{87}Sr/^{86}Sr$ ratios between 0.70331 and 0.70452. Nd model ages ($T_{DM}$) range between 1.05 and 1.17 Ga (Table 5). With respect to those of the western Anatolia Eocene–Miocene granites and Kos monzonites, plotting close or in the mantle array, all Baklan samples have a striking negative $\varepsilon_{Nd(t)}$ values (−5.0 to −5.6) (Fig. 13b). The Sr–Nd isotopic ratios plot near and subparallel to the fields for lower crustal granulite xenolithes from Lashaine and Lesotho, South Africa (Cohen et al., 1984; van Calsteren et al., 1986), showing a spread consistent with the field for Qianxi granulites from North China Block (NCB) (Jahn and Zhang, 1984) in Fig. 13c. It is note that the Menderes Massif in western Anatolia is made up of Pan-African basement and a Paleozoic to Early Tertiary cover sequence impricated by Late Alpian deformation (Hetzel et al., 1998; Candan et al., 2001).

## 7. Discussion

### 7.1. Petrogenetic implications

At first sight, the geochemical characteristics of the Baklan rocks (e.g. metaluminous, high Mg# 44–51 values, low $[Al_2O_3/(FeO + MgO + TiO_2) = (1.64–2.95)]$ and $[(Na_2O + K_2O)/(FeO + MgO + TiO_2) = (0.78–2.20)]$ ratios), together with the isotopic compositions comparable with those of lower crustal xenoliths (Figs. 11a–c and 13c), give an idea that they may be derived from the dehydration partial melting of lower crust (pure crustal melting origin). Available experimental data (e.g. Tepper et al., 1993; Roberts and Clemens, 1993; Wolf and Wyllie, 1994; Rapp and Watson, 1995) have shown that partial melting of a mafic lower crust could generate melts of metaluminous granitic composition. Alternatively, Roberts and Clemens (1993) postulated that most high-potassium, calc-alkaline, I-type granitoid magmas could be generated through partial melting of an older meta-igneous rocks in the lower crust. They are granitic to tonalitic, and result from thermal extremes in their lower crustal environments. However, the geochemical characteristics of the enclaves in Baklan granodiorite do not confirm pure crustal origin (discussed further). Granitoids having a high-K, calc-alkaline composition are characterized by enrichment in LILEs (Cs, K and Rb) and

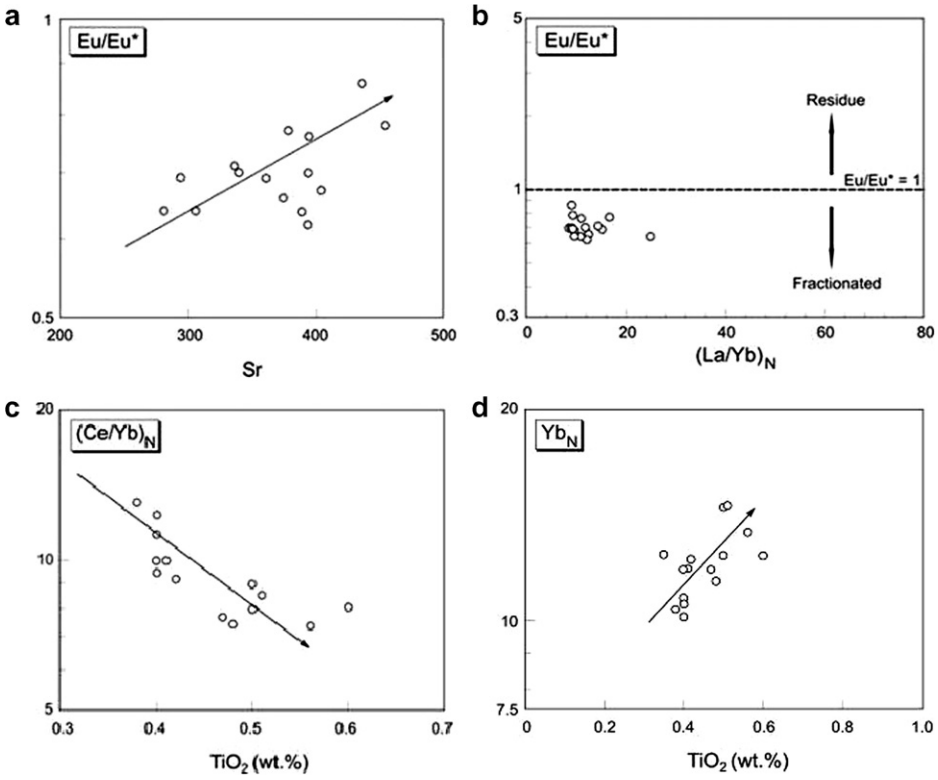


Fig. 10. (a) Plot of $Eu/Eu^*$ as measure of the negative Eu anomaly vs. Sr concentrations of Baklan Granite. (b) $Eu/Eu^*$ vs. $(La/Yb)_N$ diagram showing distribution of Baklan rocks concerning fractionation and restite trends (from Wu et al., 2005). (c) Plot of $Ce/Yb_N$ and (d) $Yb_N$ vs. $TiO_2$. Correlation between the parameters indicate strong influence of crystal fractionation processes upon REE systematics.

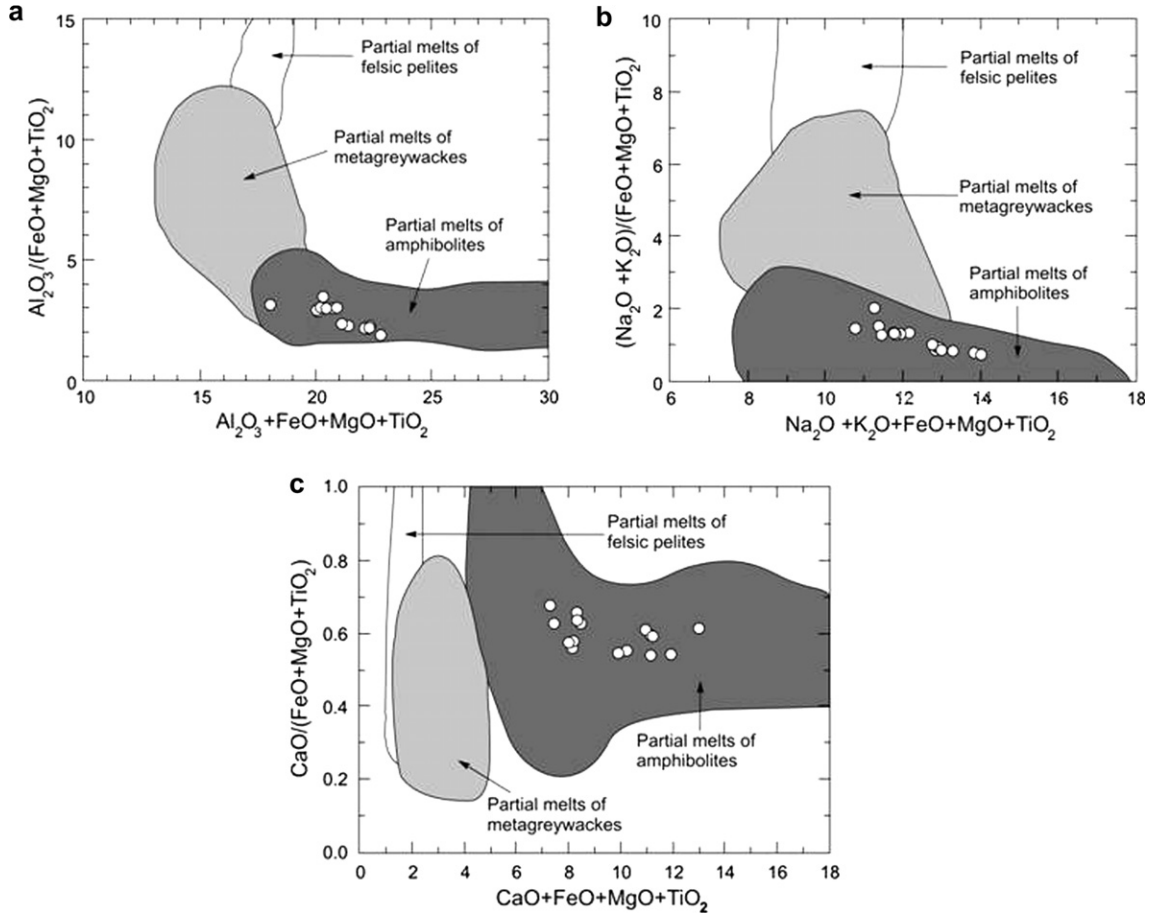


Fig. 11. (a–c) Outlined domains denote partial melting of felsic pelites, metagreywackes and amphibolites obtained in experimental studies (Patīno Douce, 1999) and compositions of representative samples from Baklan Granite.

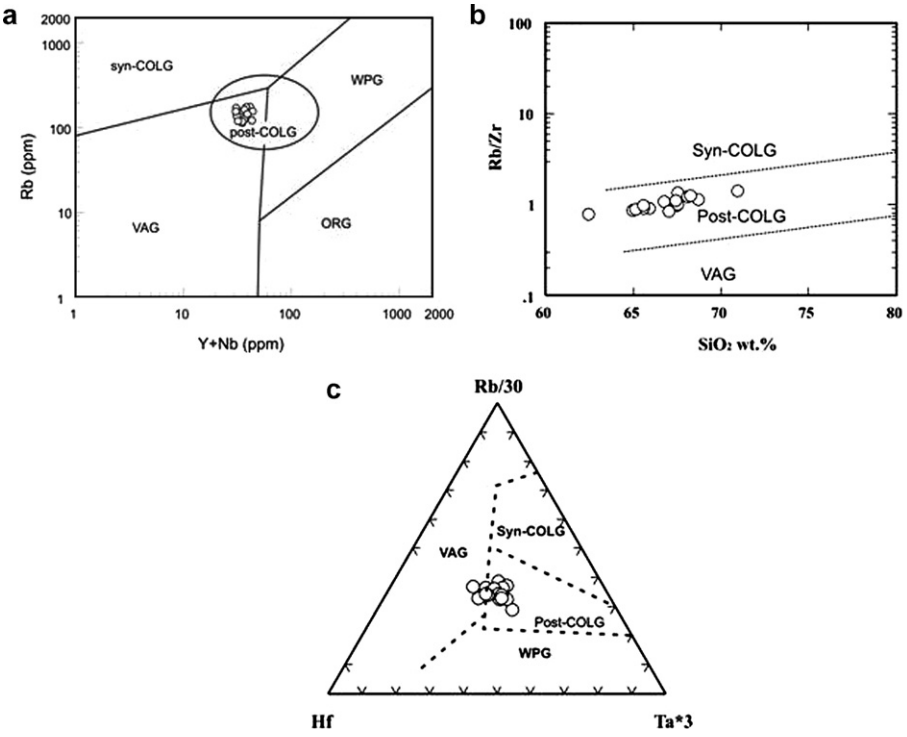


Fig. 12. (a) Updated Rb vs. (Y + Nb) discriminant diagram for granitoid tectonic setting (Pearce et al., 1984; Pearce, 1996) showing the "post-collisional" character of Baklan Granite. (b) Rb/Zr vs. $SiO_2$ discriminant diagram of Baklan rocks (Harris et al., 1986). (c) Rb–Hf–Ta discrimination diagram of Harris et al. (1986). *Key to abbreviations:* syn-collisional (Syn-COLG), Within-plate granites (WPG), Volcanic arc granites (VAG), Ocean-ridge granites (ORG).

Table 5
Sm–Nd and Rb–Sr isotopic data of Baklan Granite

| Sample number | $SiO_2$ (wt.%) | Rb (ppm) | Sr (ppm) | Rb/Sr | $^{87}Rb/^{86}Sr$ | $^{87}Sr/^{86}Sr$ | $2\sigma$ | $(^{87}Sr/^{86}Sr)_i$ | Sm (ppm) | Nd (ppm) | $^{147}Sm/^{144}Nd$ | $^{143}Nd/^{144}Nd$ | $(^{143}Nd/^{144}Nd)_i$ | $2\sigma$ | $\varepsilon_{Nd(O)}$ | $f_{Sm/Nd}$ | $\varepsilon_{Nd(t)}$ | $T_{DM}$ (Ga) |
|---|---|---|---|---|---|---|---|---|---|---|---|---|---|---|---|---|---|---|
| MBG-6 | 68.27 | 75.7 | 27.5 | 2.75273 | 7.978 | 0.705671 | 8 | 0.70352 | 4.68 | 23.9 | 0.1184 | 0.512305 | 0.512305 | 12 | −6.5 | −0.40 | −5.6 | 1.17 |
| MBG-7 | 65.12 | 64.3 | 72.8 | 0.88324 | 2.555 | 0.704528 | 8 | 0.70384 | 4.08 | 22.4 | 0.1101 | 0.512325 | 0.512325 | 11 | −6.1 | −0.44 | −5.2 | 1.05 |
| MBG-8 | 67.51 | 75.4 | 24.4 | 3.09016 | 8.933 | 0.705720 | 9 | 0.70331 | 5.79 | 30.0 | 0.1166 | 0.512336 | 0.512336 | 5 | −5.9 | −0.41 | −5.0 | 1.10 |
| MBG-11 | 62.47 | 46.5 | 175.6 | 0.26481 | 0.767 | 0.704730 | 6 | 0.70452 | 4.72 | 24.8 | 0.1149 | 0.512321 | 0.512321 | 11 | −6.2 | −0.42 | −5.3 | 1.11 |
| MBGT-1 | 64.99 | 60.2 | 80.6 | 0.74690 | 2.161 | 0.704521 | 7 | 0.70394 | 4.84 | 25.5 | 0.1148 | 0.512318 | 0.512318 | 8 | −6.2 | −0.42 | −5.4 | 1.11 |

i = calculated initial isotopic ratios. $\varepsilon_{Nd(t)} = ((^{143}Nd/^{144}Nd)_s/(^{143}Nd/^{144}Nd)_{CHUR} - 1 \times 10.000$, $f_{Sm/Nd} = (^{147}Sm/^{144}Nd)_s/(^{147}Sm/^{144}Nd)_{CHUR} - 1$, where s = sample, $(^{143}Nd/^{144}Nd)_{CHUR} = 0.512638$ and $(^{147}Sm/^{144}Nd)_{CHUR} = 0.1967$ (Jacopsen and Wasserburg, 1984).
$\lambda\ ^{147}Sm = 6.54.10^{-12}\ a^{-1}$. $^{87}Rb/^{86}Sr_{CHUR} = 0.0816$; and $^{87}Sr/^{86}Sr_{CHUR} = 0.7045$ (DePaolo, 1988).
The age of 19 My is used for $\varepsilon_{Nd(t)}$ and $(^{87}Sr/^{86}Sr)_i$ calculations; $[(^{87}Sr/^{86}Sr)_i = (^{87}Sr/^{86}Sr)_m - {}^{87}Rb/^{86}Sr\,(e^{\lambda t} - 1)$; $\lambda\ ^{87}Rb = 1.42.10^{-11}\ a^{-1}$ The model age ($T_{DM}$) is calculated using a linear isotopic ratio growth equation: $T_{DM} = 1/\lambda \times \ln(1 + ((^{143}Nd/^{144}Nd)_s - 0.5135)/((^{147}Sm/^{144}Nd)_s - 0.2137))$.
CHUR = chondritic uniform reservoir.
It is note that Rb and Sr concentration data, in here, were obtained by isotope dilution analysis (TIMS). The concentrations of Rb and Sr in Table 4 were measured by ICP-MS technique. Hence, analytical differences between Tables 4 and 5 in terms of Rb and Sr concentrations probably should result from different analytical techniques.

U and Th with respect to the HFSEs, especially Nb and Ti. Although magmas with such chemical features are consistent with those of crustal melts, trace element compositions of magmas are strongly dependent on protolith composition (e.g. Roberts and Clemens, 1993; Pearce, 1996; Förster et al., 1997) and are largely affected by progressive differentiation.

### 7.2. Significance of MME's

Mafic microgranular enclaves may provide valuable petrogenetic information on the genesis of granitic bodies (e.g. Holden et al., 1987; Pitcher, 1993; Chappell, 1996; Yang et al., 2004). Many workers supported that the enclaves represent either cognate material (residual, restitic origin) or globules of basaltic magma quenched in granitic host (mixed magmas) (e.g. Pitcher, 1993; Chappell, 1996).

As mentioned before, major elements vs. MgO variations between the host Baklan granitic rocks and their enclaves show separated trends (Fig. 7a and b). This rules out any strictly co-genetic origin, and precludes the pure crustal melting origin for this intrusion with a mantle-like Sr isotopic signature. The chemical composition of the enclave samples- BMGE-2 and BMGE-4 with high $SiO_2$ (55–59 wt.%), MgO (6.3–6.1 wt.%), Cr (308–273 ppm), Ni (69–48 ppm) and low $Al_2O_3$ (15.65–13.28 wt.%) values, probably argues for an origin from mixed source (Table 4). They may also be considered to represent remnants of a mafic component added to intermediate to felsic magma chambers (e.g. Holden et al., 1987; Didier and Barbarin, 1991; Collins, 1998). Moreover, trace element contents of some mafic enclaves (e.g. BGTA-1, BMGE-4, BMGY-1) in Baklan rocks have most characteristics of A-type granites (e.g. Whalen et al., 1987; Whalen et al., 1996). They have high Ga/Al*10000 (2.60–2.65), Zr + Nb + Y + Ce (326–355 ppm) and $Na_2O$ (2.8–4 wt.%) contents, respectively (Table 4, unshown). The enclave sample BMGE-4 displays also sharp negative Eu anomaly, which is typical of some A-type granites formed from mixing of mantle- and crustal-derived magmas (e.g. Yang et al., 2006). In terms of the Ni–Cr concentrations expected for a primitive basaltic (unfractionated) magma derived from a mantle peridotite source (e.g. Wilson, 1989) are so high (Ni > 250 ppm, Cr > 500 ppm), relatively high Cr, Ni, Sc (up to 223 ppm) and V (up to 40 ppm) contents of enclaves, together with low $Al_2O_3$ (15.65–13.28 wt.%) values equilibrated with a mantle source ($Al_2O_3 < 15$ wt.%), suggest that a mafic magma underwent a significant fractionation of olivine and pyroxene prior to mixing with the granitic end-member. Accordingly, defined hyperbolic and/or linear arrays on some selected trace element variations (e.g. Nb/Ba vs. Th/Ta, Rb/Sr vs. Y/Nb, Rb/Sr vs. La/Yb, Zr/Y vs. La/Yb, Ti/Zr vs. Yb/Hf, Fig. 14), are expected for the mixing between the two distinct compositional end-members (Fig. 14). Combined with the $T_{DM}$ data (ranging between 1.05 and 1.17 Ga) and mantle-like isotopic (low $Sr_i$) signature of Baklan rocks, it seems like that the micro-

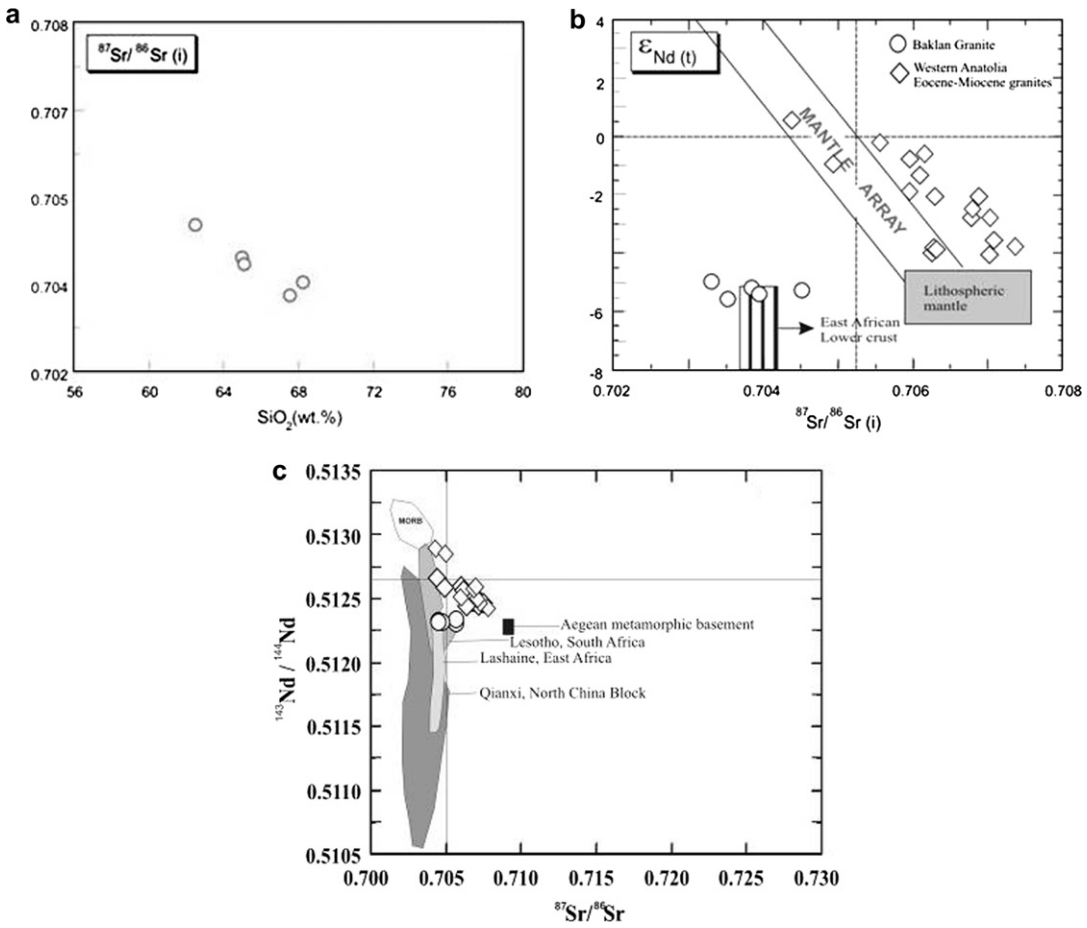


Fig. 13. Nd, Sr isotopic compositions of selected samples from Baklan Granite. (a) Initial Sr isotopic ratios vs. $SiO_2$ (wt.%). (b) Initial $\varepsilon_{Nd(t)}$ values vs. initial Sr isotopic ratios. East African lower crust (dashed field) after Cohen et al. (1984). Lithospheric end-member composition is adapted from Yang et al. (2004, 2006), as follows

| Sources | Sr (ppm) | $(^{87}Sr/^{86}Sr)_i$ | Nd (ppm) | $^{143}Nd/^{144}Nd$ | $\varepsilon_{Nd(t)}$ |
|---|---|---|---|---|---|
| Lithospheric mantle | 1070 | 0.7065 | 42 | 0.51217 | −6.0 |

(c) Comparison of Nd and Sr isotopic ratios of Baklan Granite with those of selected lower crustal granulite xenoliths. Data sources: Lashaine granulite xenoliths (East Africa), Cohen et al. (1984); Lesotho granulite xenoliths (South Africa), van Calsteren et al. (1986); Qianxi granulites from the North China Block, Jahn and Zhang (1984). MORB, Sun and McDonough (1989). Western Anatolia Eocene–Miocene granites and Kos monzonites (open diamonds) after Karacık et al. (2007), Altunkaynak (2007), Altherr and Siebel (2002) and Juteau et al. (1986). Aegean metamorphic basement is adapted from Aldanmaz et al. (2000, references therein).

granular enclaves represent additional mantle components involved in the generation of the host Baklan Granites.

In that case, we addressed the role of magma mixing in the genesis of the Baklan Granite, but source nature of Baklan pluton is associated with either (i) direct interaction between an underplated mantle-derived melt and lower crust, or (ii) partial melting of a juvenile crust.

Numerical simulations have shown that partial melting of mafic lower crust by periodic influx of basaltic magma is a viable mechanism for the generation of granitic magmas (e.g. Petford and Gallagher, 2001). The necessary heat for dehydration melting of the lower crust may be provided by a periodic influx of mantle-derived basaltic magma. Altherr and Siebel (2002),Coban and Flower (2007) and Altunkaynak (2007) suggested that additional heat was introduced from the rising asthenosphere and from basaltic underplates as a consequence of lithospheric thinning after slab-breakoff as speculated by Davies and Von Blankenburg (1995).

Recent studies in granite petrology suggested that crustal thickening as a consequences of continental collision, development of lower juvenile crust via input of mantle-derived magmas, and lithospheric thinning and asthenospheric mantle upwelling are common feature in orogenic settings (e.g. Sengor et al., 1993; Johnson, 1993; Chen and Jahn, 1998, 2004; Chen et al., 2000; Hu et al., 2000; Wu et al., 2000, 2003; Chen et al., 2002; Zhai et al., 2007; Mo et al., in press; Karsli et al., 2007). The production of extensive juvenile crust in the Central Asian Orogenic Belts is significant (Sengor et al., 1993; Jahn et al., 2000; Wu et al., 2000). Sengör et al. (1985) suggested that the crust in western Anatolia had thickened to about 50–55 km, as a result of Palaeocene orogenic contraction. It is possible that the development of a new juvenile crust during crustal

thickening as a result of collision in the Upper Cretaceous–Early Tertiary period in western Anatolia, and partial melting of this juvenile crust by influx of basaltic magma after the slab break-off could be a valid mechanism to produce the Baklan rocks under extensional tectonics.

Sr–Nd isotopic ratios of Baklan rocks and western Anatolia Eocene–Miocene granites are consistent with those of Phanareozoic lower crustal xenoliths in Europe (Fig. 15a). On the basis of $T_{DM}$ ages (1.05–1.17 Ga) and mantle-like Sr isotopic (low $Sr_i$) signatures for Baklan intrusion, it is suggested that the new juvenile crust may be a reasonable protoliths in the origin of Baklan intrusion. Accordingly, low Sr and negative Nd isotopic ratios of Baklan Granite fits lower-left quadrant of the Nd–Sr plot, expected for EM-I type source (Fig. 13b). Data that fall in the lower-left quadrant include some metasomatized mantle xenoliths (Menzies and Murthy, 1980), mafic granulites (Cohen et al., 1984), and continental basalts (Carter et al., 1978). For isotopic data from mantle-derived rocks that lie to the left of the "mantle array" (Carter et al. (1978)) suggested a source derived from mixing of a mantle-derived melt with amphibolites or granulites. All these aspects discussed above, we may have encountered a mantle source for Baklan rocks, which was LREE enriched but Rb depleted relative to Sr, similar to EMI. The parental magmas of the Baklan rocks were probably produced by partial melting of a juvenile lower crust, and the underplated mantle-derived basaltic magmas should have a geochemistry and isotopic composition similar to that of enriched mantle, with negative $\varepsilon_{Nd(t)}$ values.

In order to estimate the relative contribution of mantle-to-crust component respectively, a simple mixing model (from Yang et al., 2004) has been testified, and the result of mixing calculation using Sr–Nd isotopic data is shown in Fig. 15b and c. Fig. 15b and c demonstrates that the upper crustal component (UCC) has little or no role in the generation of the Baklan Granite; whereas mantle-derived basaltic magma and the lower crust (LCC) are the two major components. Accordingly, the higher-positive $\varepsilon_{Nd(t)}$ and low initial $^{87}Sr/^{86}Sr$ ratios for the western Anatolia Eocene–Miocene granites (e.g. Samos, Kapıdağ, Marmara, Karabiga, Sarıoluk, Gönen, Orhaneli, Topuk, Gürgenyayla) (Juteau et al., 1986; Altherr and Siebel, 2002; Karacık et al., 2007; Altunkaynak, 2007) and Kos monzonites (Altherr and Siebel, 2002), similar to those of group I granites from NE China (Wu et al., 2000), also suggest a high proportion of juvenile material in their petrogenesis (Fig. 15b and c). With respect to the Baklan rocks, they may be interprated that the granitic magma were produced by melting of a mixed lithology containing a lower crustal rocks intruded or underplated by a basaltic magma in such a proportion. Hence, we strongly suggest that the input of juvenile magmas played significant role in the source domains of western Anatolia Eocene–Miocene granites.

## 8. Conclusion

The Baklan Granite from western Anatolia is of subalkaline affinity, belong to the high-K, calc-alkaline series

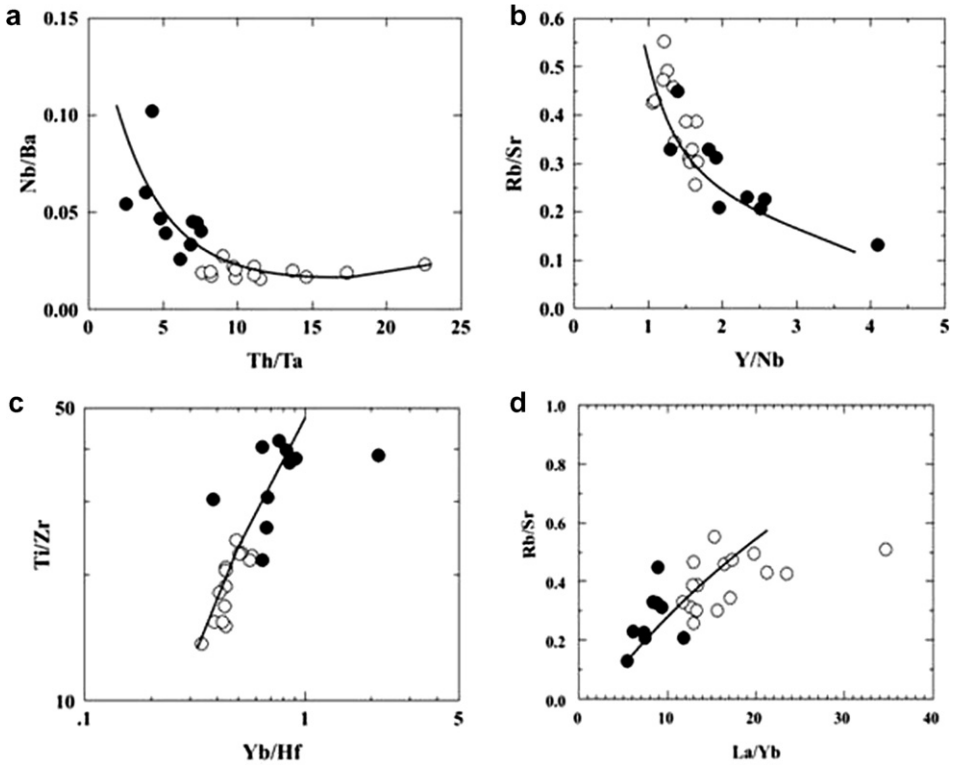


Fig. 14. Interelement ratio a) Nb/Ba vs. Th/Ta, b) Rb/Sr vs. Y/Nb, c) Ti/Zr vs. Yb/Hf, d) Rb/Sr vs. La/Yb) plots for Baklan rocks and monzonitic enclaves.

and display features typical of I-type affinity. It is classified as a post-collisional granitoid (post-COLG) in terms of parameters of tectonic setting (e.g. Pearce et al., 1984). The composition of the mafic microgranular enclaves and host rocks of the Baklan intrusion provide direct evidence for the involvement of mantle-derived juvenile magmas in their genesis. The geochemical and isotopic compositions of the Baklan granitic rocks suggest that they were generated not via partial melting of lower crustal granulitic residues, but by either (i) mixing of lithospheric mantle-derived magma with lower crustal-derived magmas, or (ii) partial melting of a (relatively) juvenile crust, which is probably a mixed lithology formed by pre-existing lower crust intruded or underplated by mantle-derived basaltic magma. Additionally, the generation of the (late syn)- post-collisional intrusions with higher $\varepsilon_{Nd(t)}$ values from the western Anatolia also require a much higher proportion of juvenil component in their source domains. It appears that a drastic change from compressional to extensional settings in western Anatolia provide an important tectonic environment for crustal melting and mantle input for the generation of (late syn)- post-collisional granitic bodies.

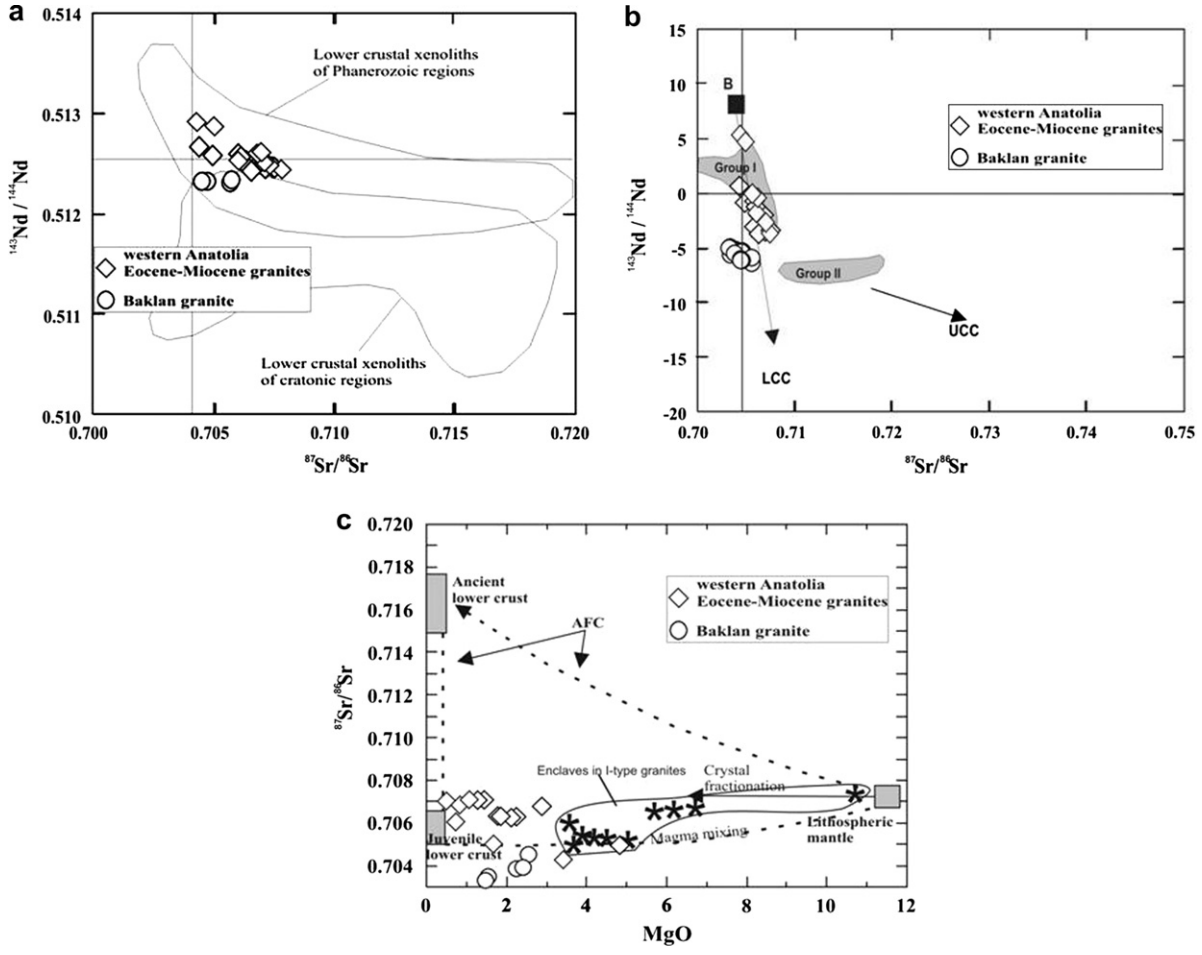


Fig. 15. (a) Comparison of Baklan Granites and western Anatolia (late syn)- post-collisional granites, with the Phanareozoic and cratonic lower crustal granulite xenoliths from Europe in $^{87}Sr/^{86}Sr$ vs. $^{143}Nd/^{144}Nd$ variation diagram. Fields adapted from Downes et al. (2001). Western Anatolia Eocene–Miocene granites (open diamonds) after Karacık et al. (2007); Altunkaynak (2007), Altherr and Siebel (2002) and Juteau et al. (1986). (b) $\varepsilon_{Nd(t)}$ vs. $^{87}Sr/^{86}Sr$ plot showing mixing proportions between two end-members: (1) juvenile components (B, basalt), and (2) crustal components (LCC, lower continental crust; or UCC, upper continental crust). The parameters used are taken from Wu et al. (2000). (c) Plots of $(^{87}Sr/^{86}Sr)_i$ vs. MgO for Baklan Granites. For comparison, western Anatolia Eocene–Miocene granites (open diamond) (Karacık et al., 2007; Altunkaynak, 2007; Altherr and Siebel, 2002; Juteau et al., 1986) are also plotted. The data for dioritic enclaves in I-type granites are from Yang et al. (2004) and Karsli et al. (2007). The calculated parameters of end-member isotope compositions (for ancient lower crust, juvenile lower crust and lithospheric mantle) and Sr concentrations in the construction of AFC and magma mixing trends are adapted from Yang et al. (2004, 2006) and are as follows

| Sources | Sr (ppm) | $(^{87}Sr/^{86}Sr)_i$ |
|---|---|---|
| Lithospheric mantle | 1070 | 0.7065 |
| Juvenile lower crust | 480 | 0.7050 |
| Ancient lower crust | 300 | 0.7200. |

## Acknowledgements

This work is a part of our project regarding poly-metallic mineralization around the Baklan Granite from the Muratdağı region, western Anatolia (Türkiye). Financial support was partly provided by the Scientific and Technical Research Council of Türkiye (TÜBİTAK; Grant #: YDA-BAG-103Y113) and a grant from the Research Foundation of Süleyman Demirel University, Türkiye (SDU; grant #: 764-D-03). We gratefully acknowledge them. We would also like to express our gratitude to Prof. Bor-ming Jahn (Universite de Rennes, France), Prof. Nilgün Güleç (Middle East Technical University, Turkey), Prof. Erdin Bozkurt (Middle East Technical University, Turkey), Prof. Erdinç Yiğitbaş (Onsekizmart University, Turkey) and Assoc. Prof. Orhan Karslı (Karadeniz Technical University, Turkey) for their helpful criticism, detailed discussions and suggestions which improved the text.

## References

Akdeniz, N., Konak, N., 1979. Simav-Emet-Tavşanlı-Dursunbey-Demirci yöresinin jeolojisi. MTA Rapor No: 6547, Ankara (in Turkish).

Albayrak, Ö., 2003. Eğrigöz Masifi kuzey ve batı kesimi (Tavşanlı/Kütahya) polimetalik cevherleşmelerinin jenetik incelemesi ve jeodinamik ortam koşullarının tanımlanması. Unpublished MSc Thesis, Dokuz Eylül University, pp. 87 (in Turkish with English abstract).

Aldanmaz, E., 2006. Mineral-chemical constraints on the Miocene calc-alkaline and shoshonitic volcanic rocks of Western Turkey: disequilibrium phenocryst assemblages as indicators of magma storage and mixing conditions. Turk. J. Earth Sci. 15, 47–73.

Aldanmaz, E., Pearce, J.A., Thirlwall, M.F., Mitchell, J.G., 2000. Petrogenic evolution of Late Cenozoic, post-collision volcanism in western Anatolia, Turkey. J. Volcanol. Geothermal Res. 102 (1–2), 67–95.

Arslan, M., Aslan, Z., 2006. Mineralogy, petrography and whole-rock geochemistry of the Tertiary granitic intrusions in the Eastern Pontides, Turkey. J. Asian Earth Sci. 27, 177–193.

Altherr, R., Siebel, W., 2002. I-type plutonism in a continental back-arc setting: Miocene granitoids and monzonites from the central Aegean Sea, Greece. Contrib. Mineral. Petrol. 143, 397–415.

Altunkaynak, Ş., 2007. Collision-Driven Slab Breakoff Magmatism in Northwestern Anatolia, Turkey. J. Geol. 115, 63–82.

Altunkaynak, Ş., Yılmaz, Y., 1998. The Mount Kozak magmatic complex, western Anatolia. J. Volcanol. Geothermal Res. 85, 211–231.

Aydoğan, M.S., 2006. Determination of metal zoning and mineral paragenesis of the base metal mineralizations around Baklan Granite (Muratdağı, Banaz/Uşak, Turkey) and their genesis by means of isotope geochemistry. PhD Thesis, Science Institute, Suleyman Demirel University, Turkey, pp. 238. (Turkish with English Abstract).

Barka, A.A., 1992. The North Anatolian Fault Zone. Ann. Tectonicae 6, 164–195.

Bingöl, E., 1977. Muratdağı jeolojisi ve ana kayaç birimlerinin petrolojisi: Türkiye Jeoloji Kurumu Bülteni 20, 13–66, in Turkish with English Abstract.

Bingöl, E., Delaloye, M., Ataman, G., 1982. Granitic intrusions in western Anatolia, a contribution to the geodynamic study of this area. Eclogae Geologicae Helvetiae 75, 437–446.

Bingöl, E., 1989. Geological map of Turkey, scale 1:2,000,000. Mineral Research and Exploration Institute Publications, Ankara, Türkiye.

Bozkurt, E., 2001a. Neotectonics of Turkey – synthesis. Geodinamica Acta 14, 3–30.

Bozkurt, E., 2001b. Late Alpine evolution of the central Menderes Massif, western Anatolia, Turkey. Int. J. Earth Sci. 89, 728–744.

Bozkurt, E., Mittwede, S.K., 2005. Introduction: evolution of continental extensional tectonics of western Turkey. Geodinamica Acta 18 (3–4), 153–165.

Boztuğ, D., Harlavan, Y., Arehart, G.B., Satir, M., Avci, N., 2007. K–Ar age, whole-rock and isotope geochemistry of A-type granitoids in the Divriği-Sivas region, Eastern-central Anatolia, Turkey. Lithos 97, 193–218.

Candan, O., Dora, Ö., Oberhansli, R., Çetinkaplan, M., Partzsch, J.H., Warkus, F.C., Dürr, S., 2001. Pan-African high-pressure metamorphism in the Precambrian basement of the Menderes Massif, western Anatolia, Turkey. Int. J. Earth Sci. 89, 793–811.

Carter, S.R., Evensen, N.M., Hamilton, P.J., O'Nions, R.K., 1978. Neodymium and strontium isotope evidence for crustal contamination of continental volcanics. Science 202, 743–746.

Catlos, E.J., Çemen, I., 2005. Monazite ages and the evolution of the Menderes Massif, western Turkey. Int. J. Earth Sci. (Geol. Rundsch) 94, 204–217.

Chappell, B.W., 1996. Magma Mixing and the Production of Compositional Variation within Granite Suites: Evidence from the Granites of Southeastern Australia. J. Petrol. 39, 449–470.

Chappell, B.W., White, A.J.R., 1974. Two contrasting granite types. Pacific Geol. 8, 173–174.

Chappell, B.W., White, A.J.R., 1992. I- and S-type granites in the Lachlan Fold Belt. Trans. R. Soc. Edinb., Earth Sci. 83, 1–26.

Chen, B., Jahn, B.-m., 1998. Crustal evolution of southeastern China: Nd and Sr isotopic evidence. Tectonophysics 284, 101–133.

Chen, J., Zhou, T., Xie, Z., Zhang, X., Guo, X., 2000. Formation of positive 1 Nd(T) granitoids from the Alataw Mountains, Xinjiang, China, by mixing and fractional crystallization: implication for Phanerozoic crustal growth. Tectonophysics 328, 53–67.

Chen, B., Jahn, B.-m., Wei, C., 2002. Petrogenesis of Mesozoic granitoids in the Dabie UHP complex, Central China: trace element and Nd–Sr isotope evidence. Lithos 60, 67–88.

Chen, B., Jahn, B.-m., 2004. Genesis of post-collisional granitoids and basement nature of the Junggar Terrane, NW China: Nd–Sr isotope and trace element evidence. J. Asian Earth Sci. 23, 691–703.

Cohen, R.S., O'Nions, R.K., Dawson, J.B., 1984. Isotope geochemistry of xenoliths from East Africa: implications for development of mantle reservoirs and their interaction. Earth Planet. Sci. Lett. 68, 209–220.

Collins, W.J., 1998. Evaluation of petrogenetic models for Lachlan Fold Belt granitoids: implications for crustal architecture and tectonic models. Austr. J. Earth Sci. 45, 483–500.

Cox, K.G., Bell, J.D., Pankhurst, E.P.L., 1979. The interpretation of igneous rocks. George Allen and Unwin, London, pp. 450.

Coban, H., Flower, M.F.J., 2007. Late Pliocene lamproites from Bucak, Isparta (southwestern Turkey): implications for mantle 'wedge' evolution during Africa-Anatolian plate convergence. J. Asian Earth Sci. 29, 160–176.

Davies, J.H., Von Blankenburg, F., 1995. Slab breakoff: a model of lithosphere detachment and its test in the magmatism and deformation of collisional orogens. Earth Planet. Sci. Lett. 129, 85–102.

Debon, F., Le Fort, P., 1983. A chemical-mineralogical classification of common plutonic rocks and associations. Trans. R. Soc. Edinb., Earth Sci. 73, 135–149.

Delaloye, M., Bingöl, E., 2000. Granitoids from western and northwestern Anatolia: geochemistry and modelling of geodynamic evolution. Int. Geol. Rev. 42, 241–268.

DePaolo, D.J., 1988. Neodymium Isotope Geochemistry: An IntroductionMinerals and Rocks, vol. 20. Springer-Verlag, Berlin, pp. 187.

Dewey, J.F., Pitman, W.C., Ryan, W.B.F., Bonnin, J., 1973. Plate tectonics and evolution of the Alpine system. Geol. Soc. Am. Bull. 84, 3137–3180.

Dewey, J.F., Hempton, M.R., Kidd, W.S.F., Şaroğlu, F., Şengör, A.M.C., 1986. Shortening of continental lithosphere; the neotectonics of Eastern Anatolia, a young collision zone. In: Coward, M.P., Ries, A.C. (Eds.), Collision Tectonics. Geological Society of London Special Publication 19, pp. 3–36.

Dias, G., Simoes, P.P., Ferreira, N., Leterrier, J., 2002. Mantle and crustal sources in the genesis of late-Hercynian granitoids (NW Portugal): geochemical and Sr–Nd isotopic constraints. Gondwana Res. 5, 287–305.

Didier, J., Barbarin, B., 1991. Enclaves and Granite PetrologyDevelopments in Petrology, vol. 13. Elsevier Science, Amsterdam, pp. 626.

Downes, H., Markwick, A.J.W., Kempton, P.D., Thirlwall, M.F., 2001. The lower crust beneath cratonic north-east Europe: isotopic constraints from garnet granulite xenoliths. Terra Nova 13, 395–400.

Emre, T., Sözbilir, H., 2007. Tectonic evolution of the Kiraz Basin, Küçük Menderes Graben: evidence for compression/uplift-related basin formation overprinted by extensional tectonics in West Anatolia. Turk. J. Earth Sci. 16, 441–470.

Ercan, T., Dinçel, A., Metin, S., Türkecan, A., Günay, E., 1978. Uşak yöresindeki Neojen havzaların jeolojisi. Türkiye Jeoloji Bülteni 21, 97–106, in Turkish with English Abstract.

Ersoy, Y., Helvacı, C., 2007. Stratigraphy and geochemical features of the Early Miocene bimodal (ultrapotassic and calc-alkaline) volcanic activity within the NE-trending Selendi Basin, Western Anatolia, Turkey. Turk. J. Earth Sci. 16, 117–139.

Förster, H.J., Tischendorf, G., Trumbull, R.B., 1997. An evaluation of the Rb vs. (Y+Nb) discrimination diagram to infer tectonic setting of silicic igneous rocks. Lithos 40, 261–293.

Genç, Ş.C., 1998. Evolution of the Bayramiç Magmatic Complex, northwestern Anatolia. J. Volcanol. Geothermal Res. 85, 233–249.

Güleç, N., 1991. Crust-mantle interaction in western Turkey: implications from Sr and Nd isotope geochemistry of Tertiary and Quaternary volcanics. Geol. Mag. 23, 417–435.

Günay, E., Akdeniz, N., Şaroğlu, F., Çağlayan, A., 1986. Murat Dağı-Gediz Dolaylarının Jeolojisi. Maden Tetkik Arama Enstitüsü Yayını, 74 pp. (in Turkish).

Güngör, T., Erdoğan, B., 2002. Tectonic significance of mafic volcanics in a Mesozoic sequence of the Menderes Massif, West Turkey. Int. J. Earth Sci. 91, 386–397.

Harris, N.B.W., Pearce, J.A., Tindle, A.G., 1986. Geochemical characteristics of collision-zone magmatism. In: Coward, M.P., Ries, A.C. (Eds.), Collision Tectonics. Geological Society of London, Special Publication, 19, pp.67–81.

Hetzel, R., Romer, R.L., Candan, O., Passchier, C.W., 1998. Geology of the Bozdag area, central Menderes massif, SW Turkey: Pan-African basement and Alpine deformation. Geol. Rundsch 87, 394–406.

Holden, P., Halliday, A.N., Stephens, WE., 1987. Neodymium and strontium isotope content of microdiorite enclaves points to mantle input to granitoid production. Nature 330, 53–56.

Hu, A., Jahn, B-m., Zhang, G., Chen, Y., Zhang, Q., 2000. Crustal evolution and Phanerozoic crustal growth in northern Xinjiang: Nd isotopic evidence. Part I. Isotopic characterization of basement rocks. Tectonophysics 328, 15–51.

Irvine, T.N., Baragar, W.R.A., 1971. A guide to the chemical classification of the common volcanic rocks. Can. J. Earth Sci. 8, 523–548.

Ishihara, S., 1977. The magnetite series and ilmenite-series granitic rocks. Mining Geol. 27, 293–305.

Işık, V., Gürsu, S., Göncüoğlu, C., Seyitoğlu, G., 2004a. Deformational and geochemical features of syn-tectonic Koyunoba and Egrigöz granitoids, western Turkey. In: Chatzipetros, A.A., Pavlides, S.B. (Eds.), 5th International Symposium on Eastern Mediterranean Geology, Thessaloniki, Greece, vol. 3, pp.1143–1146.

Işık, V., Tekeli, O., Seyitoğlu, G., 2004b. The $^{40}Ar/^{39}Ar$ age of extensional ductile deformation and granitoid intrusions in the northern Menderes core complex: implications for the initiation of extensional tectonics in western Turkey. J. Asian Earth Sci. 23, 555–566.

Jacopsen, S.B., Wasserburg, G.J., 1984. Sm–Nd isotopic evolution of chondrites and achondrites. Earth Planet. Sci. Lett. 67, 137–150.

Jahn, B.-m., Zhang, Z.Q., 1984. Archean granulite gneisses from eastern Hebei Province, China: rare earth geochemistry and tectonic implications. Contrib. Mineral. Petrol. 85, 224–243.

Jahn, B.-m., Wu, F., Chen, B., 2000. Massive granitoid generation in Central Asia: Nd isotope evidence and implication for continental growth in the Phanerozoic. Episodes 23 (2), 82–92.

Johnson, C.M., 1993. Mesozoic and Cenozoic contributions to crustal growth in the southwestern United States. Earth Planet. Sci. Lett. 118, 75–89.

Jung, S., Hoernes, S., Mezger, K., 2002. Synorogenic melting mafic lower crust: constraints from geochronology, petrology and Sr, Nd, Pb and O isotope geochemistry of quartz diorites (Damara orogen, Namibia). Contrib. Mineral. Petrol. 143, 551–566.

Juteau, M., Michard, A., Albarede, F., 1986. The Pb–Sr–Nd isotope geochemistry of some recent circum-Mediterranean granites. Contrib. Mineral. Petrol. 92, 331–340.

Karacık, Z., Yılmaz, Y., 1998. Geology of the ignimbrites and the associated volcano-plutonic complex of the Ezine area, northwestern Anatolia. J. Volcanol. Geothermal Res. 85, 251–264.

Karacık, Z., Yılmaz, Y., Pearce, J.A., Ece, I., 2007. Petrochemistry of the south Marmara granitoids, northwest Anatolia, Turkey. Int. J. Earth Sci. (Geol. Rundsch). doi:10.1007/s00531-007-0222-y.

Karsli, O., Chen, B., Aydin, F., Şen, C., 2007. Geochemical and Sr–Nd–Pb isotopic compositions of the Eocene Dölek and Sariçiçek Plutons, Eastern Turkey: Implications for magma interaction in the genesis of high-K calc-alkaline granitoids in a post-collision extensional setting. Lithos 98, 68–96.

Kaya, O., Ünay, E., Göktaş, F., Saraç, G., 2007. Early Miocene stratigraphy of Central West Anatolia, Turkey: implications for the tectonic evolution of the Eastern Aegean area. Geol. J. 42, 85–109.

Kemp, A.I.S., Hawkesworth, C.J., 2003. Granitic perspectives on the generation and secular evolution of the continental crust. In: Rudnick, R.L. (Eds.), The Crust. Treatise on Geochemistry, vol .3, pp. 349–410.

Köprübaşı, N., Aldanmaz, E., 2004. Geochemical constraints on the petrogenesis of Cenozoic I-type granitoids in Northwestern Anatolia, Turkey: evidence for magma generation by lithospheric delamination in a post-collisional setting. Int. Geol. Rev. 46, 705–729.

Maniar, P.D., Piccoli, P.M., 1989. Tectonic discrimination of granitoids. Bull. Am. Geol. Soc. 101, 635–643.

McKenzie, D., 1972. Active tectonics of the Mediterranean Region. Geophys. J. R. Astronom. Soc. 30, 109–185.

McKenzie, D., 1978. Active tectonics of the Alpine–Himalayan belt: the Aegean sea and surrounding regions. Geophys. J. R. Astronom. Soc. 55, 217–254.

Mendes, A.C., Dias, G., 2004. Mantle-like Sr–Nd isotope composition of Fe–K subalkaline granites: the Peneda–Geres Variscan massif (NW Iberian Peninsula). Terra Nova (16/3), 109–115.

Menzies, M., Murthy, V.R., 1980. Enriched mantle: Nd and Sr isotopes in diopsides from kimberlite nodules. Nature 283, 634–636.

Mo, X., Hou, Z., Niu, Y., Dong, G., Qu, X., Zhao, Z., Yang, Z., in press. Mantle contributions to crustal thickening during continental collision: evidence from Cenozoic igneous rocks in southern Tibet. Lithos.

Okay, A.İ., Tansel, İ., Tüysüz, O., 2001. Obduction, subduction and collision as reflected in the Upper Cretaceous–Lower Eocene sedimentary record of western Turkey. Geol. Mag. 138, 117–142.

Okay A.İ., Satır, M., Siyako, M., Monie, P., Metzger, R., Akyüz, S., 1996. Paleo- and Neo-Tethyan events in northwestern Turkey: geologic and geochronologic constrains. In: Yin A, Harrison TM (Eds.), The Tectonic Evolution of Asia, 420–441.

Patīno Douce, A.E., 1999. What do experiments tell us about the relative contributions of crust and mantle to the origin of granitic magmas? In: Castro, A., Fernandez, C., Vigneressese, J.L. (Eds.), Understanding Granites: Integrating New and Classical Techniques. Geological Society of London, Special Publication, vol. 168, pp.55–75.

Pe-Piper, G., Piper, D.J.W., 2001. Late Cenozoic, post-collisional Aegean igneous rocks: Nd, Pb and Sr isotopic constraints on petrogenetic and tectonic models. Geol. Mag. 138 (6), 653–668.

Pearce, J.A., Harris, N.B.W., Tindle, A.G., 1984. Trace element discrimination diagrams for the tectonic interpretation of granitic rocks. J. Petrol. 25, 956–983.

Pearce, J.A., 1996. Sources and settings of granitic rocks. Episodes 19, 120–125.

Petford, N., Gallagher, K., 2001. Partial melting of mafic (amphibolitic) lower crust by periodic influx of basaltic magma. Earth Planet. Sci. Lett. 193, 483–499.

Pitcher, W.S., 1993. The Nature and Origin of Granite. Blackie Academic & Professional, pp. 321.

Rapp, R.P., Watson, E.B., 1995. Dehydration melting of metabasalt at 8–32 kbar: implications for continental growth and crust-mantle recycling. J. Petrol. 36, 891–931.

Rickwood, P.C., 1989. Boundary lines within petrologic diagrams which use oxides of major and minor elements. Lithos 22, 247–263.

Roberts, M.P., Clemens, J.D., 1993. Origin of high-potassium, calc-alkaline, I-type granitoids. Geology 21, 825–828.

Shand, S.J., 1927. Eruptive Rocks. D. Van Nostrand Company, New York, pp. 360.

Snyder, D.B., Lucas, S.B., McBride., J.H., 1996. Crustal and mantle reflectors from Palaeoproterozoic orogens and their relation to arc-continent collisions. Geological Society, London, Special Publications 112, pp. 1–23.

Streckeisen, A., Le Maitre, R.W., 1979. A chemical approximation to the modal QAPF classification of the igneous rocks. Neues Jahrbuch für Mineralogie, Abhandlungen 136, 169–206.

Sun, S.S., McDonough, W.F., 1989. Chemical and isotopic systematics of oceanic basalts: implications for mantle composition and processes. In: Saunders, A.D., Norry, M.J. (Eds.), Magmatism in Ocean Basins. Geological Society of London, Special Publication, vol. 42, pp.313–345.

Şengör, A.M.C., 1980. Principles of the neo-tectonics of Turkey. Geological Society of Turkey, pp. 40.

Sengör, A.M.C., Yılmaz, Y., 1981. Tethyan evolution of Turkey: a plate tectonic approach. Tectonophysics 75, 181–241.

Sengör, A.M.C., Görür, N., Şaroğlu, F., 1985. Strike slip faulting and related basin formation in zones of tectonic escape: Turkey as a case study. In: Biddle, T.R., Christic-Blick, N. (Eds.), Strike-slip Deformation, Basin Formation and Sedimentation. Society of Economic Paleontologist and Mineralogists, Special Publication, vol. 37, pp.227–264.

Sengor, A.M.C., Natal'in, B.A., Burtman, V.S., 1993. Evolution of the Altaid tectonic collage and palaeozoic crustal growth in Eurasia. Nature 364, 299–307.

Tepper, J.H., Nelson, B.K., Bergantz, G.W., ft Irving, A.J., 1993. Petrology of the Chilliwack batholith, North Cascades, Washington: generation of calc-alkaline granitoids by melting of mafic lower crust with variable water fugacity. Contrib. Mineral. Petrol. 113, 333–351.

Tirel, C., Gueydan, F., Tiberi, C., Brun, J.-P., 2004. Aegean crustal thickness inferred from gravity inversion. Geodynamical implications. Earth Planet. Sci. Lett. 228, 267–280.

Topuz, G., Altherr, R., Schwarz, W.H., Siebel, W., Satir, M., Dokuz, A., 2005. Post-collisional plutonism with adakite-like signatures: the Eocene Saraycık granodiorite (Eastern Pontides, Turkey). Contrib. Mineral. Petrol. 150, 441–455.

van Calsteren, P.W.C., Harris, N.B.W., Hawkesworth, C.J., Menzies, M.A., Rogers, N.W., 1986. Xenoliths from southern Africa: a perspective on the lower crust. In: Dawson, J.B., Carswell, D.A., Hall, J., Wedepohl, K.H. (Eds.), The Nature of the Lower Continental Crust. Geol. Soc. Spec. Publ., vol. 24, pp. 351– 362.

Whalen, J.B., Currie, K.L., Chappell, B.W., 1987. A-type granites: geochemical characteristics, discrimination and petrogenesis. Contrib. Mineral. Petrol. 95, 407–419.

Whalen, J., Jenner, G.A., Longstaffe, F.J., Robert, F., Gariepy, C., 1996. Geochemical and Isotopic (O, Nd, Pb and Sr) Constraints on A-type Granite Petrogenesis Based on the Topsails Igneous Suite, Newfoundland Appalachians. J. Petrol. 37, 1463–1489.

Wilson, M., 1989. Igneous Petrogenesis Kluwer, Dordrecht , 450 pp.

Wolf, M.B., Wyllie, J.P., 1994. Dehydration melting of amphibolite at 10 kbar: the reflects of temperature and time. Contrib. Mineral. Petrol. 115, 369–383.

Wu, F.Y., Jahn, B-m., Wilde, S.A., Sun, D-.Y., 2000. Phanerozoic crustal growth: U ± Pb and Sr ± Nd isotopic evidence from the granites in northeastern China. Tectonophysics 328, 89–113.

Wu, F.Y., Jahn, B-m., Wilde, S.A., Lo, C.-H., Yui, T.-Z., Lin, Q., Ge, W.-C., Sun, D.-Y., 2003. Highly fractionated I-type granites in NE China (II): isotopic geochemistry and implications for crustal growth in the Phanerozoic. Lithos 67, 191–204.

Wu, F.Y., Yang, J.H., Wilde, S.A., Zhang, X.O., 2005. Geochronology, petrogenesis and tectonic implications of Jurassic granites in the Liaodong Peninsula, NE China. Chem. Geol. 221, 127–156.

Yang, J.-H., Wu, F.-Y., Chung, S.-L., Wilde, S.A., Chu, M.-F., 2004. Multiple sources for the origin of granites: geochemical and Nd/Sr isotopic evidence from the Gudaoling granite and its mafic enclaves, northeast China. Geochim. Cosmochim. Acta 68 (21), 4469–4483.

Yang, J.-H., Wu, F.-Y., Chung, S.-L., Wilde, S.A., Chu, M.-F., 2006. A hybrid origin for the Qianshan A-type granite, northeast China: geochemical and Sr–Nd–Hf isotopic evidence. Lithos 89, 89–106.

Yılmaz, Y., 1997. Geology of western Anatolia. In: Schindler, C., Pfister, M. (Eds.), Active tectonics of Northwestern Anatolia – the Marmara Poly-Project. A multidisciplinary approach by Space-Geodesy, Geology, Hydrogeology, Geothermics and Seismology, VDF Hochschulverlag an der ETH, Zürich, pp. 31–53.

Zhai, M., Fan, Q., Zhang, H., Sui, J., Shao, J., 2007. Lower crustal processes leading to Mesozoic lithospheric thinning beneath eastern North China: underplating, replacement and delamination. Lithos 96, 36–54.